# Design, synthesis and biological evaluation of novel pyrazolo-pyrimidin-amines as potent and selective BTK inhibitors*

Darshan Joshi [a,b], Rajesh Bahekar [a,*], Shubhangi Soman [b], Pradip Jadav [a], Dipam Patel [a], Amitgiri Goswami [a], Jignesh Pethani [a], Jeevan Kumar [a], Jitendra Patel [a], Rajesh Sundar [a], Poonamgiri Goswami [a], Krishnarup Goshdastidar [a], Hoshang Patel [a], Ankit Patel [a], Debdutta Bandyopadhyay [a], Abhijit Chattarjee [a], Manoranjan Sharma [a], Mukul Jain [a], Ranjit Desai [a]

[a] Department of Medicinal Chemistry, Zydus Research Centre, Sarkhej-Bavla, N.H. 8A Moraiya, Ahmedabad 382210, India
[b] Department of Chemistry, Faculty of Science, The Maharaja Sayajirao University of Baroda, Vadodara 390002, India

## ARTICLE INFO

## ABSTRACT

To discover the best-in-class Bruton's Tyrosine Kinase (BTK) inhibitors, for th treatment of autoimmune disorders like cancer (B-Cell Lymphoma (BCL)) and rheumatoid arthritis (RA), in the present investigation, novel structural optimizations were carried out. Introduction of novel bicyclic amine linkers and aromatic backbone led to series of compounds 9a-h and 14a-u. Compound 14b was found to be potent, orally bioavailable, selective and irreversible BTK inhibitor. *In vitro*, 14b showed IC$_{50}$ of 1.0 nM and 0.8 nM, in BTK and TMD8 assays, respectively. *In vivo*, 14b displayed robust efficacy in collagen-induced arthritis (CIA) and TMD8 xenograft models, which could be correlated with its improved oral bioavailability. In the repeated dose acute toxicity study, 14b showed no adverse changes, indicating that the BTK inhibitor 14b could be viable therapeutic option for the treatment of autoimmune disorders.

## 1. Introduction

BTK is a cytoplasmic tyrosine kinase of TEC family. It is the second largest family of non-receptor kinase, in human [1]. BTK signals many type of cell surfaces molecules and it is mainly expressed in B cell, macrophages and monocytes [2]. B cell maturation, differentiation and proliferation were mainly regulated by B cell receptor (BCR), where in, role of BTK enzyme is very crucial [3]. In BCR pathway, BTK is activated by the upstream Src-family kinase, such as Blk, Lyn and Fyn. In turn, BTK phosphorylate and activates phospholipase Cgamma2 (PLCγ2), leading to Ca$^{+2}$ mobilization and activation of NF-$_k$B and MAP kinase pathways which are essential for B cell survival [4]. Immune cells like mast cell, basophils, monocytes, macrophages play important roles in inflammatory and allergic responses. Constitutive BTK activation under autoimmune conditions leads to activation of Fc receptor of IgG and IgE (FcγR, FcεR), in macrophages and mast cells [5].

BTK has been shown to play key role in several auto-immune disorders like lupus, RA, multiple sclerosis (MS) and various types of B-cell malignancies (mantle cell lymphoma (MCL), chronic lymphocytic lymphoma (CLL) or small lymphocytic lymphoma (SLL)). Thus, inhibition of BTK is considered as the most validated and persuade target for the effective treatment of auto-immune disorders [6–12]. In last decade, intense efforts been made to develop selective BTK inhibitors, especially against closely associated cysteine kinases such as EGFR, JAK3, BLK, BMX and TEC, for the safe and effective treatment of autoimmune disorders [13–15].

Ibrutinib (IBR) is the first generation orally administered BTK inhibitor which covalently binds to Cys481 of active adenosine triphosphate (ATP) binding domain of a BTK enzyme [16]. IBR was approved by FDA, in 2013 to treat mantle cell lymphoma (MCL) and was subsequently approved for various indications, such as chronic lymphocytic leukemia (CLL), waldenstrom's macroglobulinemia (WM), and marginal

zone lymphoma [17]. However, IBR not only irreversibly binds to BTK but also induces off-target inhibitions of multiple cysteine kinases. Off-target binding of IBR associated with various adverse effects (AEs), such as bleeding, rash, diarrhea, fungal infection, neutropenia and atrial fibrillation (AF), which may lead to treatment discontinuation. Further to achieve clinical efficacy, high doses (420–560 mg, q.d) of IBR is needed, due to its poor pharmacokinetic (PK) profile (<3% oral bioavailability (%F), in humans, with variable exposure) [18]. IBR exposure also get impacted by concomitant CYP3A inhibitors and hepatic impairment, which led to potential safety concerns [19]. Long-term treatment with IBR led to resistance (−60 %), caused by the development of mutated clones (C481S), in the IBR binding site [20].

Acalabrutinib and Zanubrutinib are the second generation irreversible BTK inhibitors which has been approved by FDA, for the treatment of MCL [21,22]. Acalabrutinib covalently binds to C481 in the BTK, with an IC$_{50}$ of 3 nM. It has less off-target binding and a much higher specificity for BTK than IBR. In contrast to IBR, Acalabrutinib does not inhibit the TEC-family kinases (ITK and TXK), ERBB2, and Src-kinases (Src, Lyn, Fyn, Yes and Lck); however, it inhibits the epidermal growth factor receptor (EGFR), which led to diarrhea and rashes [23]. Acalabrutinib has a shorter half-life than IBR and is given twice daily. In general, cardiovascular events were less common in the Acalabrutinib group compared to IBR [24].

Zanubrutinib exhibit enhanced selectivity for BTK and improved bioavailability relative to IBR. Zanubrutinib demonstrated potent activity and selectivity against BTK over TEC, EGFR, and Src families. Zanubrutinib showed comparable-to-improved efficacy, superior safety, with lower incidences of AF, hypertension, diarrhea and bleeding. These clinical observations are in consistence with less off-target inhibition of Zanubrutinib, including ERBB2/HER2 and ERBB4/HER4 (AF), EGFR (diarrhea) and TEC (AF, bleeding). Among the approved BTK inhibitors, Zanubrutinib is less prone to modulations of its PK by intrinsic and

extrinsic factors, including food, and hepatic impairment as well as DDI, with strong or moderate CYP3A inhibitors. Compared to approved doses of 420 or 560 mg QD for IBR and 100 mg BID for Acalabrutinib, Zanubrutinib doses of 320 mg QD or 160 mg BID provides additional dosing flexibility and increased drug adherence to maximize therapeutic benefits [25].

Other irreversible BTK inhibitor like Tirabrutinib (for BCL), Evobrutinib (for MS), Branebrutinib (for RA, Systemic lupus erythematosus (SLE) and Stevens-Johnson syndrome (SJS)), Orelabrutinib (for B-cell malignancies and autoimmune diseases) are in clinical development (Fig. 1). Reversible BTK inhibitors, Fenebrutinib (for RA and SLE) and Rilzabrutinib (for immune thrombocytopenia (ITP)) are also in the clinical development [12,26–28]. However, there is still an unmet need to develop safe, potent and selective BTK inhibitors, for the effective treatment of autoimmune disorders.

## 2. Design of novel pyrazolo-pyrimidin-amine derivatives

Covalent inhibition of kinases by targeting a non-catalytic cysteine residue is a validated strategy for achieving sustained target engagement, without requiring high systemic drug exposure [29,30]. In BTK enzyme structure, Cys481 is proximal to the ATP binding site, and an analogous cysteine residue is present in few other human kinases. The relatively low prevalence of the corresponding cysteine residue in the human kinome makes covalent inhibition of BTK an attractive strategy for achieving high selectivity [31]. Pyrazolo[3,4-d]pyrimidin-4-amine and its mimetic scaffold are known for its kinase inhibitory activities.

Based on the co-crystal structure of IBR with BTK enzyme (Fig. 4), IBR structure can be categorized into four parts: hinge binder, amine linker, aromatic backbone, and warhead. The hinge binder (pyrazolo [3,4-d]pyrimidin-4-amine) forms hydrogen bonding with the Met477 (at hinge region) and Glu475, in the active site of BTK. These
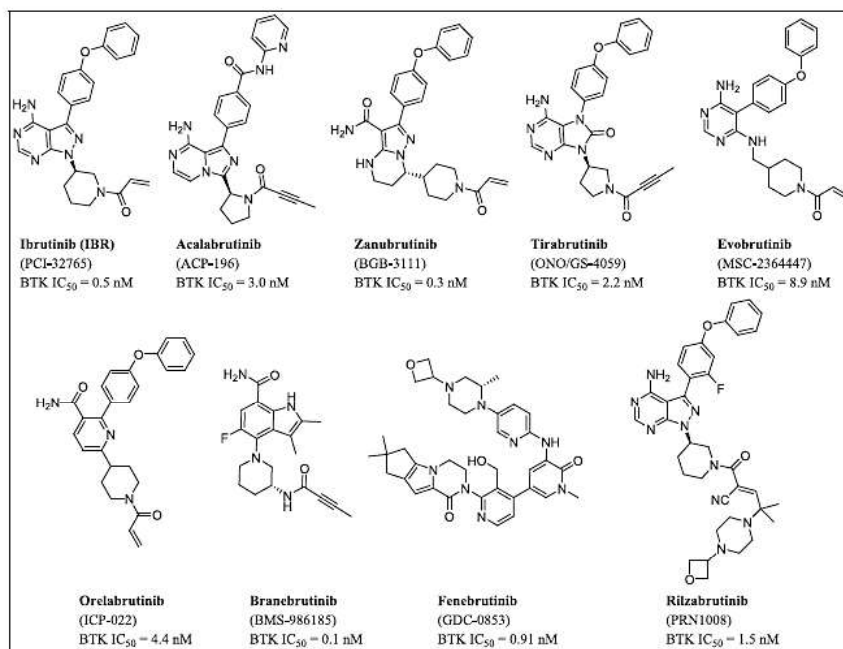


Fig. 1. Representative chemical structures of covalent and non-covalent BTK inhibitors.

interactions are very crucial for the BTK inhibitory activity. While piperidine amine acts as a linker and provides spatial angle so that warhead (acrylamide moiety) can interact covalently with Cys481. Aromatic backbone (biphenyl ether) orients towards the back side pocket of Thr474 and exhibit π-π stacking interactions with the Phe540 of a BTK enzyme.

The crucial hinge binder pyrazolo[3,4-d]pyrimidin-4-amine core was considered as a starting point. In the present investigation, stepwise structural modifications were carried out in the **IBR** (Fig. 1) to discover novel, potent, selective and orally bioavailable BTK inhibitor. Initially, to improve BTK enzyme selectivity, while retaining potency, first set of compounds were designed to identify the novel amine linker. Subsequently, to optimize aromatic backbone and warhead moiety, second and third set of compounds were designed. Thus, in the present communication, we reported design, synthesis and biological evaluation

of novel, potent and selective pyrazolo[3,4-d]pyrimidine-4-amine based irreversible BTK inhibitors.

## 3. Result and discussion

### 3.1. Chemistry

Synthesis of pyrazolo[3,4-d]pyrimidine based derivatives (9a-h and 14a-u) were carried out as depicted in Scheme 1, 2 and 3, following the modified literature procedure [32]. For the synthesis of 9a-h (Scheme 1), commercially available (ethoxymethylene)malononitrile (1) reacted with hydrazine hydrate to get 5-amino-1H-pyrazole-4-carbonitrile (2), which was converted to 1H-pyrazolo[3,4-d]pyrimidin-4-amine (3) by reacting with formamide. Intermediate 3 was iodinated using *N*-iodo succinimide to get an iodo intermediate 4, which was subjected for
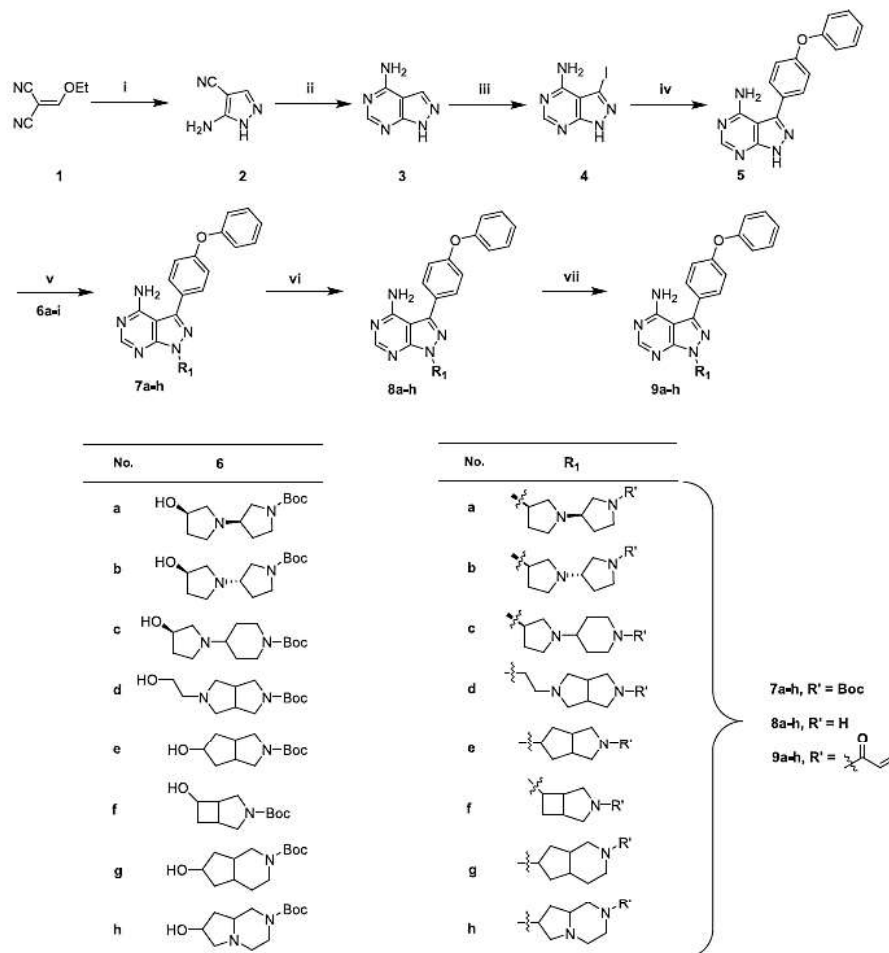


Scheme 1. Synthetic route of Compounds 9a-h. Reagents and conditions: i) Hydrazine hydrate, 110 °C, 3 h; ii) Formamide, 180 °C, 5 h; iii) NIS, DMF, 80 °C, 18 h; iv) 4-phenoxyphenyl boronic acid, PdCl₂(PPh₃)₂, KHCO₃(aq), DMF, 90 °C, 5 h; v) 6a-h, DIAD, PPh₃, THF, 0 °C to r.t, 18 h; vi) TFA, DCM, 0 °C to r.t, 3 h; vii) Acrolyl chloride, DIPEA, DCM, 0 °C to r.t,18 h.
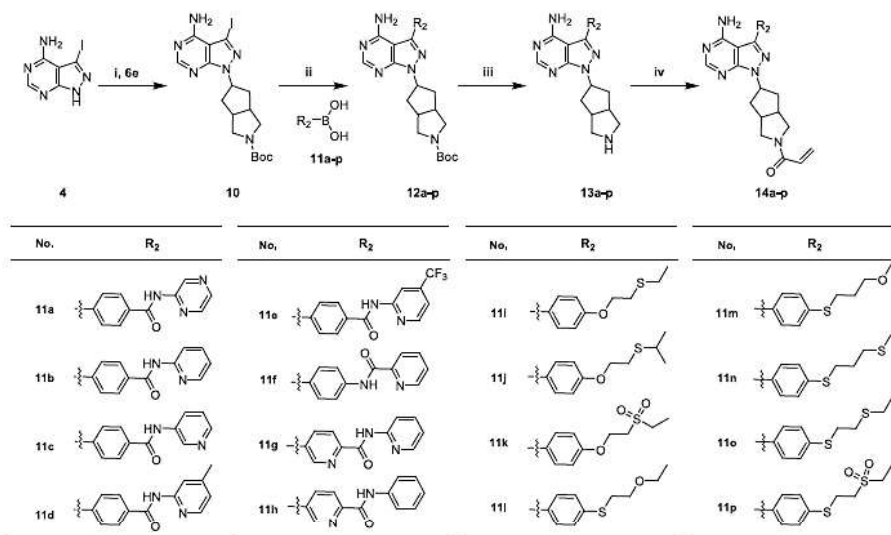
**Scheme 2.** Synthetic route of compounds 14a-p. Reagents and conditions: i) DIAD, PPh₃, THF, 0 °C to r.t, 18 h; ii) R₂-boronic acid, PdCl₂(PPh₃)₂, KHCO₃(aq), DMF, 90 °C, 5 h; iii) TFA, DCM, 0 °C to r.t, 3 h; iv) Acrolyl chloride, DIPEA, DCM, 0 °C to r.t,18 h.
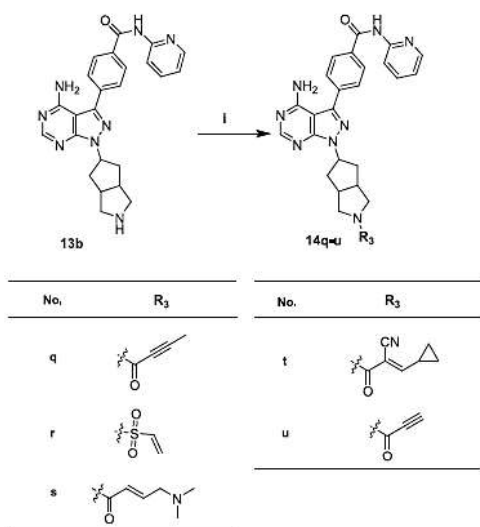


**Scheme 3.** Synthetic route of compounds 14q-u. Reagents and conditions: i) R₃-Acyl chloride,TEA, DCM, 0 °C to r.t, 3 h. or R₃-Acid, HBTU, DIPEA, DMF, 0 °C to r.t,18 h.

palladium catalyzed Suzuki-Miyaura coupling reaction, with (4-phenoxyphenyl)boronic acid to get the 3-(4-phenoxyphenyl)-1H-pyrazolo [3,4-d]pyrimidin-4-amine (5). Further Mitsunobu reaction of 5 was carried out with various substituted alcohol 6a-h [33], in the presence of diisopropylazodicarboxylate and triphenyl phosphine to get

intermediates 7a-h. Tert-butyl carbamate group of 7a-h was deprotected using trifluoroacetic acid, followed by acylation with acryloyl chloride, in the presence of base to obtain compounds 9a-h, with good yield and purity.

To synthesize 14a-p (Scheme 2), iodo intermediate (4) converted to intermediate 10, using 6e, under Mitsunobu condition, followed by coupling with various substituted boronic acid (11a-p), using palladium catalyzed Suzuki Miyaura cross coupling reaction condition to get an intermediate 12a-p. Tert-butyl carbamate group of intermediates 12a-p was deprotected, using trifluoroacetic acid, followed by acylation of intermediates 13a-p, using acryloyl chloride, in the presence of base to get 14a-p. Synthetic route for the preparation of 14q-u was displayed in Scheme 3. Intermediate 13b was coupled with substituted acyl chloride or with substituted acid, using coupling reagent to provide targeted compound 14q-u.

Overall, 29 compounds (9a-h and 14a-u) were prepared under the mild reaction conditions with > 95 % purity. Spectral data of all the synthesized compounds were found to be in conformity with the structures assigned, which ensure the formation of the compounds 9a-h and 14a-u (see experimental section 5.2. for analytical data).

### 3.2. Biological evaluation

#### 3.2.1. In vitro BTK inhibitory and anti-proliferative activity

All the synthesized compounds were assessed for their *in vitro* BTK inhibitory activity, using a cell-free biochemical assay. Briefly, fixed amount of recombinant purified human BTK (3 ng/reaction) was incubated with increasing concentration of test compounds. Enzymatic reaction was initiated by adding a substrate cocktail containing ATP (50 μmol/L), in 96 well plates. The reaction was incubated at room temperature, for 2 h followed by quantification of the left over ATP, according to the manufacturer's protocol, using ADP-Glo reagent. Data were plotted taking 'enzyme with no inhibitor' as the 100 % kinase.

Anti-proliferative activity of test compounds were evaluated *in vitro* in the human diffuse large B cell lymphoma (DLBCL) cell line TMD8. Briefly, defined numbers of TMD8 cells were incubated in 96 well plates

with increasing concentration of test compounds. Cell growth was measured using MTT assay and $IC_{50}$ values were determined by nonlinear regression, using the GraphPad Prism 6 software. IBR was taken as the positive control and it showed $IC_{50}$ of 1.1 nM and 1.2 nM, in BTK and TMD8 assay, respectively.

**Identification of a novel amine linker:** Saturated bicyclic amines were introduced as bioisosteric replacement of amine linker and overall, eight compounds (9a-h) were synthesized in this series. Test compounds were screened in both the *in vitro* assays (Table 1). All the test compounds (9a-h) displayed single digit nanomolar activity ($IC_{50}$), in BTK and TMD8 assay, except 9c (pyrrolidine piperidine linker) and 9f (azabicyclo heptane linker), which showed weaker potency, in both the *in vitro* assays. Among 9a and 9b (diastereomers, with bipyrrolidine linkers), 9b (RS) showed potent BTK inhibitory and anti-proliferative activity ($IC_{50}$: 2.8 nM and 1.4 nM, respectively) compared to 9a (RR). Compounds 9g (cyclopentyl pyridine linker) and 9h (pyrrolo pyrazine linker) showed similar ($IC_{50}$: – 3 nM) activities, indicates that there is no impact of bridgehead nitrogen, in 9h, on *in vitro* activity. Compound 9d (pyrrolo pyrrole ethyl linker) showed moderate activity. Among 9a-h, the best amine linker was found to be cyclopentyl pyrrole analogue 9e. It showed BTK inhibitory ($IC_{50}$: 1.4 nM) and anti-proliferative activity ($IC_{50}$: 0.5 nM) comparable to IBR. Thus, in our initial attempts, we could successfully replace piperidine linker of IBR with novel cyclopentyl pyrrole linker (9e), without compromising *in vitro* potency.

To further scrutinize biologically, 9e was subjected for CYP, hERG inhibitory activity and PK study (Tables 4 and 5). As depicted in Table 4, 9e showed <50 % inhibition of hERG and CYP (1A2, 2C9, 2D6, 2C19, and 3A4), at 10 μM concentration. The PK study in mice and rats reveals that 9e have slightly better PK profile ($C_{max}$ = 282 and 283 ng/mL, AUC = 433 and 301 ng.h/mL, %F = 36 and 25, in mice and rats, respectively) compare to IBR (see Table 5). Thus the promising *in vitro* and PK data of 9e encouraged us to further optimize its aromatic backbone.
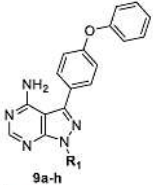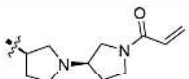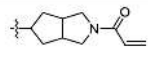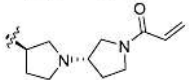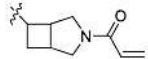
**Optimization of aromatic backbone:** Preliminary docking study

data of 9e suggested that an aromatic backbone of 9e adopt favorable orientation in the hydrophobic pocket of BTK enzyme, which allows it to interact with the key residues (Thr474 and Phe540) of hydrophobic pocket (Fig. 4). Docking study also revealed that if we introduce a hydrogen bond acceptor in aromatic backbone, additional hydrogen bond interactions may occur with the Ser538 or/and Lys430, which could lead to kinase selectivity. Based on these finding, we selected two set of aromatic backbone bioisosteres. In the first set, benzamide / picolinamide derivatives were selected, while in the second set, 4-phenyl ether/ thioether derivatives were used as aromatic backbone bioisosteres. Total sixteen compounds (14a-p) were synthesized and evaluated in BTK and TMD8 assays. The results of both *in vitro* assays are summarized in the Table 2.
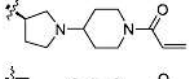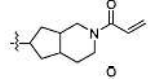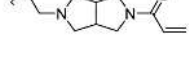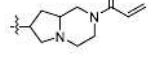
In the first set, compounds with benzamide / picolinamide backbone (14a-h) displayed potent BTK inhibitory activity and anti-proliferative effect in *in vitro* assays. Among 14a-e, N-2-pyridyl compounds (14b, 14d and 14e) were found to be most potent, in both the assays, with $IC_{50}$ value ≤ 1 nM. When N-2-pyridyl (14b) was replaced with N-2-Pyrazine (14a) or N-3-pyridine (14c), it showed four to five fold weaker BTK inhibitory activity and anti-proliferative effect. Reverse amide (14f) and picolinamide derivatives (14g-h) were found to be slightly inferior compared to benzamide derivatives, in both the assays.
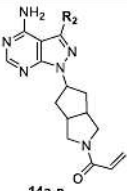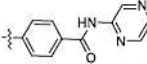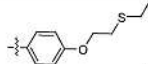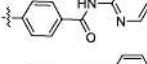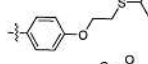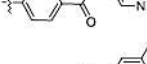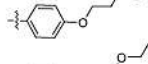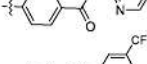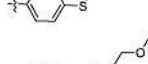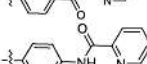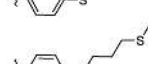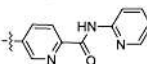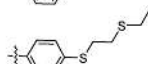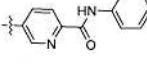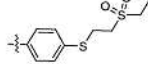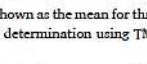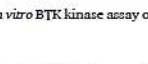
Thus, among eight compounds tested, in benzamide series, position of nitrogen in ring B (14b, 14d and 14e) was found to be crucial for potent *in vitro* activity. Also substitution with methyl (14d) or electron withdrawing group such as $CF_3$ (14e), at 5th position of pyridyl ring (ring B) was found to be favorable. The Log P value of 14b was found to be 2.7 and it increases to 3.19 and 3.62 in 14d and 14e, respectively, which indicates that all the three compounds more likely to have optimal physicochemical and ADME properties for oral dosing. Introduction of additional nitrogen at 5th position (14a) or changing the nitrogen from 2nd to 3rd position (14c), in ring-B lead to moderate activity and also decrease in the Log P, 1.37 and 1.99, for 14a and 14c,

**Table 1**
Identification of novel amine linker, *in vitro* data of 9a-h.



| Comp. | R₁ | BTK $IC_{50}$ (nM)[a] | TMD8 $IC_{50}$ (nM)[b] | Comp. | R₁ | BTK $IC_{50}$ (nM)[a] | TMD8 $IC_{50}$ (nM)[b] |
|---|---|---|---|---|---|---|---|
| 9a | | 5.1 | 4.4 | 9e | | 1.4 | 0.5 |
| 9b | | 2.8 | 1.4 | 9f | | 29 | 21 |
| 9c | | 38 | 46 | 9g | | 2.9 | 2.8 |
| 9d | | 8.1 | 11 | 9h | | 3.6 | 3.3 |
| IBR | | 1.1 | 1.2 | | | | |

All the data are shown as the mean for three experiments. [a]BTK inhibition ($IC_{50}$) determination using *in vitro* BTK kinase assay on ADP Glo platform, [b]TMD8 cytotoxicity inhibition ($IC_{50}$) determination using TMD8 cell lines assay.

5

**Table 2**
Optimization of aromatic backbone, *in vitro* data of 14a-p.



14a-p

| Comp. | R$_2$ | BTK IC$_{50}$ (nM)[a] | TMD8 IC$_{50}$ (nM)[b] | Comp. | R$_2$ | BTK IC$_{50}$ (nM)[a] | TMD8 IC$_{50}$ (nM)[b] |
|---|---|---|---|---|---|---|---|
| 14a | | 4.4 | 4.3 | 14i | | 8.3 | 8.8 |
| 14b | | 1.0 | 0.8 | 14j | | 14.6 | 7.5 |
| 14c | | 4.0 | 3.9 | 14k | | 89 | 82 |
| 14d | | 0.6 | 0.4 | 14l | | 9.4 | 8.5 |
| 14e | | 0.6 | 0.2 | 14m | | 10.4 | 10.8 |
| 14f | | 8.1 | 7.2 | 14n | | 0.8 | 1.7 |
| 14g | | 7.5 | 7.1 | 14o | | 0.8 | 0.4 |
| 14h | | 7.6 | 7.8 | 14p | | 18.9 | 13.7 |
| | IBR | 1.1 | 1.2 | | | | |

All the data are shown as the mean for three experiments. [a]BTK inhibition (IC$_{50}$) determination using *in vitro* BTK kinase assay on ADP Glo platform, [b]TMD8 cytotoxicity inhibition (IC$_{50}$) determination using TMD8 cell lines assay.

respectively. Similarly, reverse amide 14f and introduction of additional nitrogen in ring-A (14g and 14h) was found to be less favorable for *in vitro* activity.

In set 2, eight compounds (14i-p) were synthesized using phenyl ether/ thioether as aromatic backbone. Phenyl ether analogues 14i, 14j and 14k showed weaker BTK inhibitory activity (IC$_{50}$: 8.3 nM, 14.6 nM and 89 nM, respectively) and anti-proliferative effect (IC$_{50}$: 8.8 nM, 7.5 nM and 82 nM, respectively), indicates that phenyl ether linkage is not favorable. However, phenyl thioether analogues (14n and 14o) were found to be highly potent in both the BTK (IC$_{50}$: 0.8 and 0.8 nM, respectively) and TMD8 assay (IC$_{50}$: 1.7 and 0.4 nM, respectively). Compounds 14l and 14m displayed moderate inhibitory activity, in both the assays, while 14p was found to be least potent. Overall in this set, only methyl-thio (14n) and ethyl-thio (14o) analogs retained BTK inhibitory activity over alkyl-sulfonyl or alkoxy derivatives. Potent BTK inhibitory activity of 14n and 14o (lacking ring B and amide component) was found to be contradictory with our previous benzamide series (set 1) observations, having additional aryl amide (ring B) as an aromatic backbone, which we thought as an essential component for H-

bonding and hydrophobic interactions with the hydrophobic pocket of BTK enzyme.

Compounds 14b, 14d, 14e, 14n, and 14o having IC$_{50}$ ≥ IBR were screened for hERG and CYP inhibitory activity (Table 4). Tested compounds (14b, 14d, 14n and 14o) showed <50 % inhibition of hERG, at 10 μM concentration, except 14e, which showed 63 % inhibition. CYP inhibition study data reveals that phenyl thio-ether analogue 14n and 14o inhibits multiple CYP isoforms (>50 % inhibition of 2C8, 2C9, 2D6 and 2C19), at 10 μM concentration. Whereas, benzamide analogues 14b showed no CYP liabilities (<50 % inhibition), at 10 μM concentration, while 14d and 14e showed > 50 % inhibition of 2C9, at 10 μM concentration. In general, CYP inhibition has also been correlated to increased molecular weight (MW) and lipophilicity [34]. Among 14b, 14d and 14e, only 14b was found to be devoid of CYP liability, which could be correlated with its low MW and Log P. Compounds 14n and 14o exhibit higher Log P (3.63 and 3.86, respectively) and lower basicity compared to 14b, which may accounts for multiple CYP inhibitions.

Warhead influence: Electrophilic warheads part of designed BTK

inhibitors covalently interacts with nucleophilic Cys481 of BTK enzyme. With conventional acrylamide warhead, **14b** was found to be highly potent (BTK and TMD8 assay IC$_{50}$ of 1.0 and 0.8 nM, respectively) and devoid of hERG and CYP liabilities (<50 % inhibition, at 10 μM concentration). Further to probe warhead influence on *in vitro* activity, selected Michael acceptors (R$_3$, Table 3), as warheads were used, in place of acrylamide and five compounds **14q-u** were synthesized.

SAR study around various α, β-unsaturated amide groups reveals that among five different warheads selected, only 2-butenamide (**14q**) matched with the acrylamide (**14b**), in the BTK and TMD8 assay, with IC$_{50}$ of 1.2 nM and 0.9 nM, respectively. Favorable butenamide warhead is also present in the Acalabrutinib and Tirabrutinib, with pyrrolidine linker. Other Michael acceptors **14r** (vinyl sulfonamide), **14s** (dimethyl aminomethyl amide) and **14u** (2-propioloyl amide) displayed four to six fold less potency in both the *in vitro* assays, while **14t** (cyno cyclopropyl acrylamide) showed poor BTK inhibitory and anti-proliferative effect. In CYP and hERG inhibitory studies, **14q** showed <50 % inhibition for all CYP isoenzymes and hERG inhibition, at 10 μM concentration (Table 4).

Thus, it has been observed that only acrylamide and butenamide warheads containing compounds (**14b** and **14q**) retained potent BTK inhibitory activity. This could be due to cyclopentyl pyrrole linker, which may provide optimal spatial angle, specifically with these two warheads only so that these warheads can interacts covalently with Cys481. It appears that extended warheads such as dimethyl amino methyl amide (**14s**), cyno cyclopropyl acrylamide (**14t**) and 2-propioloyl amide (**14u**) are not favorable with cyclopentyl pyrrole linker, which could be due to extra spacing imparted by cyclopentyl pyrrole linker.

### 3.2.2. PK profiling of 9e, 14b and 14q

Compounds **9e**, **14b** and **14q** displayed excellent *in vitro* activity and

**Table 3**
Influence of warhead on *in vitro* activity (**14q-u**).



| Comp. | R$_3$ | BTK IC$_{50}$ (nM)$^a$ | TMD8 IC$_{50}$ (nM)$^b$ |
|---|---|---|---|
| 14q | | 1.2 | 0.9 |
| 14r | | 4.9 | 3.9 |
| 14s | | 5.2 | 4.7 |
| 14t | | >100 | 83 |
| 14u | | 6.2 | 5.8 |

All the data are shown as the mean for three experiments. $^a$BTK inhibition (IC$_{50}$) determination using *in vitro* BTK kinase assay on ADP Glo platform, $^b$TMD8 cytotoxicity inhibition (IC$_{50}$) determination using TMD8 cell lines assay.

were found to be devoid of CYP and hERG liabilities. So all the three compounds were subjected for *in vivo* PK study in male BALB/c mice and Wister rats. In a single dose PK studies (3 mg/kg, po and 1 mg/kg, iv) of compounds **9e**, **14b**, **14q** and IBR, various PK parameters (Tmax, Cmax, t$_{1/2}$, Cl, AUC and %F) were recorded (Table 5). Compound **9e** and **14q** showed moderate AUC, due to its high clearance, which resulted into overall low bioavailability (25 to 37 %).

The absolute oral bioavailability (%F) of **14b** (3 mg/kg) in mice was found to be 47 %, with C$_{max}$ of 703 ng/mL, at 0.25 h (T$_{max}$), AUC of 590 ng·h/mL and half-life (t$_{1/2}$) of 0.76 h. The %F of **14b** in rats was found to be 75 %, with C$_{max}$ of 650 ng/mL, AUC of 908 ng·h/mL and t$_{1/2}$ of 2.2 h. Thus, among the compounds tested, **14b** demonstrated comparatively better PK profile than **9e**, **14q** and IBR.
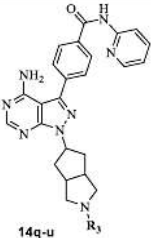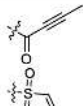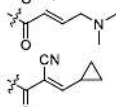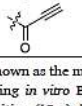
### 3.2.3. In vivo efficacy studies

#### 3.2.3.1. Antitumor activity of 14b in TMD8 xenograft model.
Based on prominent *in vitro* profile and PK properties, **14b** was selected for *in vivo* studies. To validate *in vitro* anti proliferative effect of **14b**, in *in vivo* system, anti-tumor potential of **14b** was assessed in TMD-8 DLBCL xenograft tumor-bearing mice [35]. Animals were treated with 1.5, 3, & 15 mg/kg, BID, of **14b**, for 20 days, via oral route of administration. The tumor volume was measured as described in the experimental section 5.7.1. **14b** showed dose dependent tumor growth inhibition (10 %, 50 %, and 88 %, respectively, Fig. 2).The growth inhibitory property of **14b** was more prominent after 7 days and onwards. We also compared the efficacy of **14b** (12.5 mg/kg) against IBR (12.5 mg/kg) for its antitumor activities. Our results demonstrated that **14b** had slightly better potency compared to IBR (Fig. 2), at same dose. It is important to note that **14b** does not have any effect on the body weight of the animals, during 20 days treatment (Fig. 2). Thus, the *in vivo* study validates antitumor potential of **14b**.

#### 3.2.3.2. Anti-arthritic efficacy of test compounds in collagen induced arthritis (CIA) mice model.
Arthritis was developed in male DBA1j mice, using collagen mixture and mice were recruited for the study once clinical signs were visible [36]. Ten animals were assigned in each of the three groups [vehicle, positive control (IBR, mg/kg) and test compound **14b** (0.5 mg/kg)]. Treatment was continued for four weeks, once daily and percentage inhibition in clinical score was recorded [41]. Also, to check dose dependent anti arthritic activity, doses of 0.125, 0.25, 0.5, and 1 mg/kg of **14b** were administered orally, once daily, for 28 days. The study results indicated that **14b** was far more *in vivo* efficacious compare to IBR. **14b** (0.5 mg/kg) caused 93 % reduction in clinical score while IBR (0.6 mg/kg) showed only 40 % reduction in clinical score, in the CIA model. **14b** efficacy was found to be dose related, as reduction of clinical score were 22 %, 61 %, 93 %, and 97 %, per doses of 0.125, 0.25, 0.5, & 1 mg/kg, respectively (Fig. 3).

As shown in Fig. 3, treatment with **14b** significantly suppressed the progression of disease; 0.25 mg/kg of **14b** once daily was lowest dose which showed improvement in clinical sign of disease after two days of initial dosing. The Inflammation and damage to the paw were also assessed histologically. Treatment with **14b** displayed reduction in the paw swelling based on lower histologic severity scores in the **14b** treated groups compared with the vehicle control. The paws from vehicle treated control group had a group mean severity of 10.4, while the mean severity scores in the **14b** treated mice were 5, 3.75, 1, and 0.2 at dosages of 0.125, 0.25, 0.5, & 1 mg/kg, respectively (Fig. 3). Body weights of the animals were also recorded 3 times a week as a measure of treatment related side effect. No changes in the mice body weight was observed in any treatment group, compared to vehicle control group (Fig. 3). Thus improved PK of **14b** justifies its potent *in vivo* efficacy in the CIA mice model.

7

Table 4

CYP and hERG inhibitory activity of 9e, 14b, 14d, 14e, 14n, 14o, 14q, and IBR.

| Comp. | %hERG Inhibition[a] @ 10µM | % CYP Inhibition[b] @ 10µM | | | | | |
|---|---|---|---|---|---|---|---|
| | | CYP1A2 | CYP2C8 | CYP2C9 | CYP2D6 | CYP2C19 | CYP3A4 |
| 9e | 54 | 14 | 16 | 40 | 19 | 9 | 8 |
| 14b | NI | NI | 12 | 19 | 17 | 1 | 12 |
| 14d | 26 | 13 | 27 | 63 | 34 | 27 | 2 |
| 14e | 63 | NI | 63 | 79 | 27 | 38 | 33 |
| 14n | 32 | 18 | 75 | 79 | 60 | 63 | 63 |
| 14o | 44 | 12 | 72 | 58 | 69 | 50 | 40 |
| 14q | 23 | NI | NI | 28 | 15 | 18 | 16 |
| IBR | 35 | NI | 81 | 86 | 31 | 39 | 55 |

[a] In the automated patch clamp assay. [b] incubated test compound with human liver microsomes and NADPH in the presence of CYP specific substrate, value are mean of three repeat experiment.

Table 5

Pharmacokinetic profile[a] of 14b, 14q, 9e and IBR.

| Dose | Parameters | 14b | | 14q | | 9e | | IBR | |
|---|---|---|---|---|---|---|---|---|---|
| | | Mice | Rat | Mice | Rat | Mice | Rat | Mice | Rat |
| IV 1 mg kg^{-1} | AUC (ng.h/mL) | 422 | 479 | 270 | 236 | 401 | 370 | 151 | 250 |
| | Vss (L/kg) | 0.70 | 0.88 | 0.70 | 0.54 | 0.90 | 1.37 | 0.50 | 1.50 |
| | CL (ml/min/kg) | 39.5 | 36.0 | 44.3 | 42.1 | 48.1 | 49.9 | 27.5 | 66.3 |
| | $T_{1/2}$(h) | 0.40 | 0.60 | 0.29 | 0.31 | 0.35 | 0.39 | 0.20 | 0.40 |
| PO 3 mg kg^{-1} | $T_{max}$ (h) | 0.25 | 0.25 | 0.25 | 0.25 | 0.25 | 0.25 | 0.25 | 0.25 |
| | $C_{max}$ (ng/mL) | 703 | 794 | 368 | 396 | 282 | 283 | 402 | 129 |
| | AUC (ng.h/mL) | 588 | 1074 | 300 | 219 | 433 | 301 | 277 | 86 |
| | $T_{1/2}$(h) | 0.80 | 2.00 | 0.67 | 0.80 | 0.56 | 1.08 | 0.30 | 0.80 |
| | %F* | 47 | 75 | 37 | 31 | 36 | 25 | 15 | 11 |

[a] In male BALB/c mice and male Wister rats (n = 3), test compounds were administered orally (po) at 3 mg/kg dose and plasma concentration was analyzed by LC-MS, values indicate Mean. * Oral bioavailability (%F) was calculated wrt to iv AUC. Test Compounds were administered at 1 mg/kg dose.

### 3.2.4. Kinase selectivity of 14b

BTK is among the 11 kinases (TEC, SRC and EGFR family) having cysteine residue at the structurally equivalent position, in the ATP binding domain. For additional profiling studies, 14b was evaluated for kinase selectivity, in biochemical enzyme inhibition assay and $IC_{50}$ values (Table 6) were determined. Screening of a panel of 13 different kinases demonstrated that 14b is highly selective for BTK and TEC, while for other tyrosine kinases namely ITK, FGR, HCK and JAK3, 14b were found to be 350 times less potent. Overall, 14b was found to be more BTK and TEC selective.

TEC, BTK, ITK and BMX belongs to the non-receptor tyrosine kinase families. Several BTK inhibitors showed potent binding affinity to TEC, which is expressed in CLL cells at similar levels as BTK, suggesting that concomitant binding to both of these kinases could contribute to the anti-tumor effect. On the other hand, binding to both BTK and TEC in platelets is related to bleedings, as an adverse effect of BTK inhibitors treatment [37]. Since 14b showed similar binding affinity for BMX and TEC, 14b was subjected for BMX and TEC inhibitory activity in cellular assay, using BMX and TEC NanoBRET target engagement intracellular kinase assay [38]. In BMX and TEC NanoBRET kinase assay, 14b showed <10 % inhibition at 1 µM concentration ($EC_{50}$ (Tracer 4, BMX / TEC) = >1 µM), indicates that potent binding affinity of 14b for BMX and TEC in biochemical assay does not translate in to cellular assay. Similar observations reported earlier for some other BTK inhibitors, wherein biochemical assay data do not correlate with cellular assay result. For example, in the biochemical assay, Acalabrutinib showed potent TEC inhibitory activity ($IC_{50}$: 37 nM). However, in a TEC phosphorylation assay (using human platelets), Acalabrutinib does not inhibit TEC up to non-pharmacological concentration of > 1 µM (<25 % of TEC phosphorylation at 1 µM concentration) [21]. Overall, *in vitro* selectivity of 14b against BMX and TEC in cellular assay also justify that *in vivo* anti-arthritic efficacy and antitumor activity of 14b mainly associated with selective BTK inhibition.

### 3.2.5. Safety profile of 14b

To assess the safety profile of 14b, repeat dose acute toxicity studies (14 days) was carried out in male Wistar rats (100 mg/ kg, po, once daily) and various parameters such as gross pathology, clinical signs, body weight, organ weight, serum chemistry and hematological changes were recorded. Daily oral administration of compounds 14b (33X of $ED_{50}$ dose (3 mg/kg, in CIA model)), over a period of 2 weeks did not affect the survival of Wistar rats and also no adverse changes related to gross pathology, clinical signs, body weight and feed consumption were noticed, compared to control group (Fig. 5). As shown in Tables 7 and 8, the hematological parameters of compounds 14b were found to be comparable to that of control animals. Similarly, compound 14b showed no significant changes in the serum hepatotoxicity assessment parameters as compared to the control group. Also compound 14b treated groups showed no changes in the key organs (heart, kidney, spleen and brain) weights (Fig. 6).

### 3.3. Docking study

The molecular docking analysis of 14b, 9e and IBR was carried out using CovDock [39], as shown in the Fig. 4. The covalent docking program was developed by Schrödinger, which mimics the multi-step binding process of covalent modifiers by simulating both pre- and post-reactive states. The crystal structure of the BTK enzyme (PDB ID: 5P9M) was obtained from the protein data bank and the protein structure was prepared using protein preparation wizard module of Schrödinger. For docking study, the ligands were minimized by applying an OPLS-AA force field, using ligprep module of Schrödinger [40].

The overlay of binding poses of 14b (Azure) and IBR (Salmon pink) in the BTK active site is shown in Fig. 4. As observed with IBR, amino group of pyrimidine ring of 14b forms H-bonding with backbone carbonyl of Glu474, while pyrimidine ring nitrogen form H-bonding with the backbone NH of Met477, at hinge region of BTK domain. Both IBR and 14b showed key interactions with the thiol group of Cys481 of
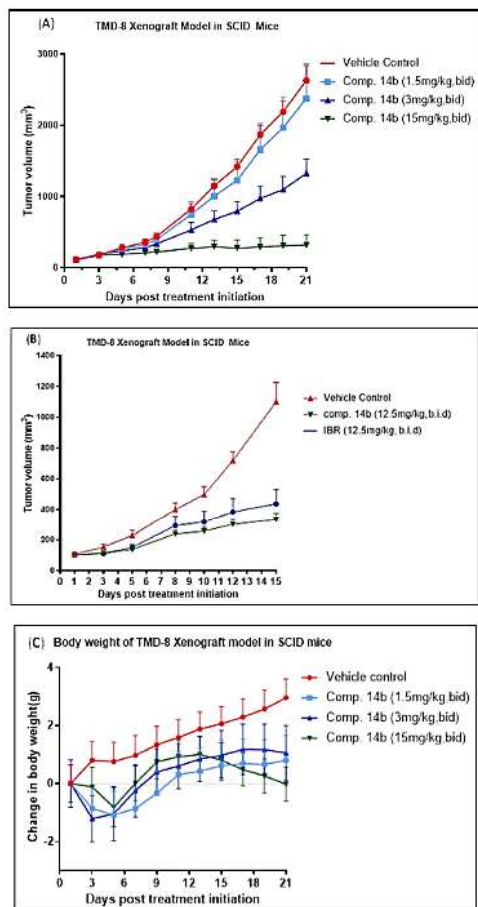
8

**Fig. 2.** *In vivo* Anti tumor activities (A) Suppression of tumor volume in TMD8 DLBCL xenograft model by 14b. Mice with established tumor reaching around 100 mm³ were divided into different groups of 10 mice each. Groups were untreated vehicle (triangle) or treated with 14b [1.5 (square), 3 (triangle) & 15 mg/kg (inverted triangle), BID] for 20 consecutive days. The data represents the mean tumor volume. (B) Suppression of tumor volume in TMD8 DLBCL xenograft model by 14b and IBR. Mice with established tumor reaching around 100 mm³ were divided into different groups of 10 mice each. Groups were untreated vehicle or treated with 14b or IBR (12.5 mg/kg, BID) for 14 consecutive days. The data represents the mean tumor volume. (C) Effects of 14b on body weight of mice treated in TMD8 DLBCL xenograft model. Mice with established tumor reaching around 100 mm³ were divided into different groups of 10 mice each. Groups were untreated vehicle or treated with 14b (1.5, 3 & 15 mg/kg, p.o, BID) for 20 consecutive days. The data represents the mean body weight. Error bars represent SEM. *, P < 0.05 when compared with vehicle control.

BTK, binds covalently as Michael adducts. The pyridine ring of benzamide interacts with Phe540 through 'T' shape π-π stacking. Overall 14b and IBR binds with active domain of BTK enzyme with the same orientation, which validated its *in vitro* BTK inhibitory activity. An additional interactions of 14b with the Ser538 and Gln412, in the
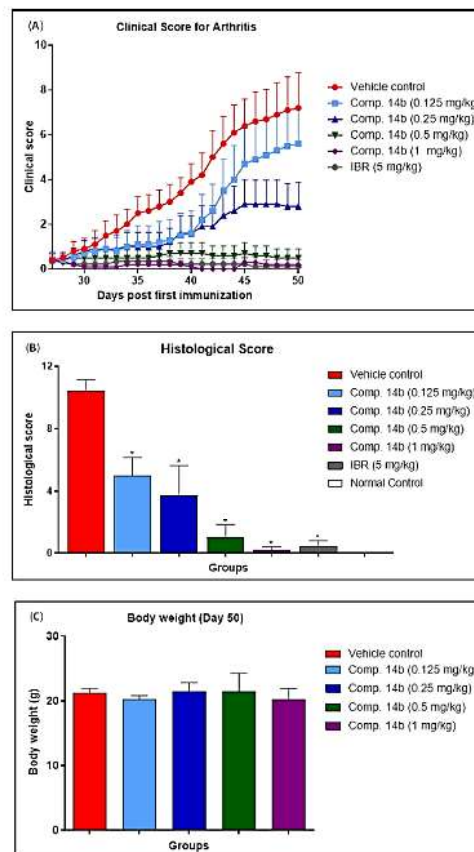


**Fig. 3.** *In vivo* anti-arthritic activities (A) Clinical score and (B) Histological score in collagen-induced arthritis (CIA) model. Mice with established CIA were divided into separate groups consisting of 10 mice each. Groups were treated vehicle (circle) or 14b [0.125(square), 0.25 (triangle), 0.5 (inverted triangle) & 1 mg/kg (diamond), OD] for 28 consecutive days. The data represent the mean arthritic or histological scores. (C) Effect of 14b on body weight after three weeks of treatment in collagen-induced arthritic mice model. Mice with established CIA were divided into separate groups consisting of 10 mice each. Groups were treated vehicle or 14b (0.125, 0.25, 0.5 & 1 mg/kg, OD) for four weeks. The data represent the mean body weight. Error bars represent SEM. *, P < 0.05 when compared with vehicle control.

catalytic domain of BTK enzyme likely to contribute towards its potent and selective BTK inhibitory activity. The docking score for IBR, 9e and 14b was found to be −11.08, −11.15 and −11.89 kcal mol⁻¹ respectively.

## 4. Conclusion

In summary, we described discovery and characterization of novel pyrazolo-pyrimidin-amine based irreversible BTK inhibitor, 14b. Stepwise structural modifications were carried out in the IBR to discover novel, potent, selective and orally bioavailable BTK inhibitor. Initially, to improve BTK enzyme selectivity, while retaining its potency, novel
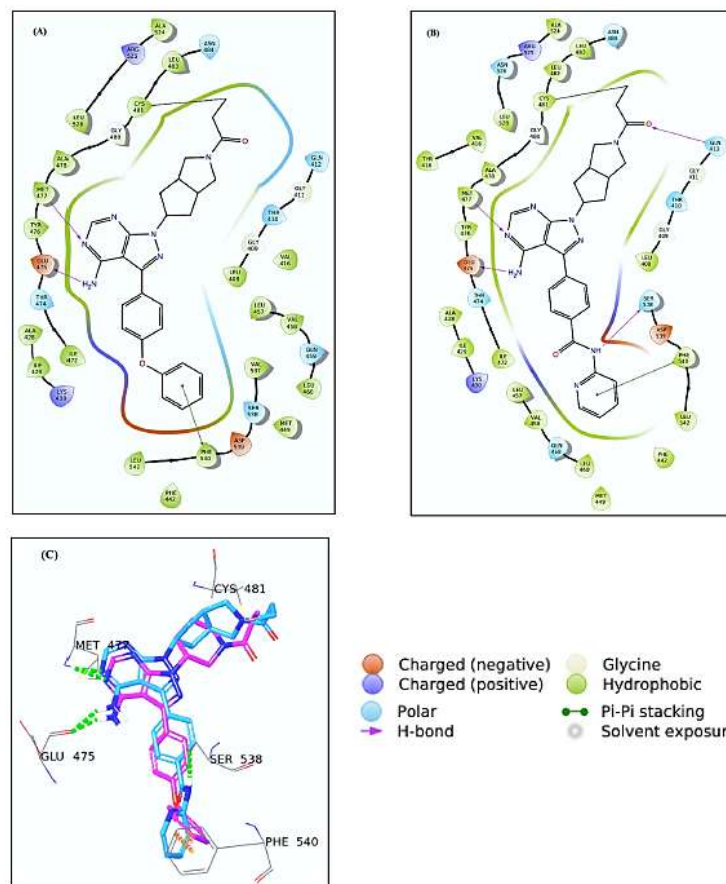
Fig. 4. Docked pose of IBR, 9e and 14b in ATP active binding sites of BTK enzyme (PDB ID: 5P9M). (A) 2D ligand interaction diagram of 9e and (B) 2D ligand interaction diagram of 14b, with residue within 5 A°, hydrogen bonds & π-π interaction are shown with arrows and lines respectively. (C) Docked pose of IBR and 14b superimposed (IBR is shown in with salmon pink coloured, while 14b is displayed with Azure coloured), green & orange dashed lines shows the hydrogen bonds interactions and π-π interaction respectively. (For interpretation of the references to colour in this figure legend, the reader is referred to the web version of this article.)

**Table 6**
Biochemical kinase selectivity of 14b.

| Kinases | IC$_{50}$ (µmol/L)[a] 14b |
|---|---|
| BTK | 0.027–0.041 |
| ITK | 18–24 |
| JAK3 | >10 |
| TEC | 0.025–0.038 |
| ERBB2 wt | 1.7–2.3 |
| EGF-R wt | 2.3–3.5 |
| BLK | 1.1–2.2 |
| BMX | 0.091–0.12 |
| ERBB4 | 0.12–0.19 |
| EGFRT790M | 4.2–5.7 |
| FGR | 10–13 |
| FRK | 1.3–1.7 |
| HCK | >10 |

[a] IC$_{50}$ values with range found from three independent experiments.

bicyclic amine based linkers were introduced. Subsequently, aromatic backbone (amide/ether) and warhead moieties were optimized rationally to establish SAR. Bioisosteric replacement with saturated bicyclic amines led to an identification of a single digit nM potent BTK inhibitor 9e, with a moderate PK profile. Further structure–activity relationship (SAR) studies with aromatic backbone (amide/ether bioisosteres) resulted in to the discovery of 4-(1-(2-acryloyloctahydrocyclopenta[c] pyrrol-5-yl)-4-amino-1H-pyrazolo[3,4-d]pyrimidin-3-yl)-N-(pyridin-2-yl)benzamide (14b).

Compound 14b displayed potent *in vitro* BTK inhibitory activity and anti-proliferation activity, which translated to the promising anti-arthritic efficacy in animal models of RA and robust antitumor activity, in TMD8 xenograft model. 14b displayed excellent *in vitro* BTK selectivity, over closely associated cysteine kinase and also it was found to be devoid of CYP and hERG liabilities. In the repeat dose acute toxicity study, 14b showed no adverse changes related to gross pathology, clinical signs and liver toxicity. Based on pre-clinical profile, compound 14b was nominated as an IND candidate, ZYBT1. Additional profiling studies, such as *in vitro* irreversible binding with BTK, inhibitory activity in C581S mutant, cytotoxic potential, using a battery of cell

10

**Fig. 5.** Body weight of rats during treatment of 14b (100 mg/kg/day). Values expressed as mean: $n = 5$, Male and female Wister rats, vehicle = Tween-80 + 0.5 % Methyl Cellulose (1:99), administered through oral gavage route.

**Table 7**
Hematological parameters after two weeks treatment of 14b (100 mg/kg/day).

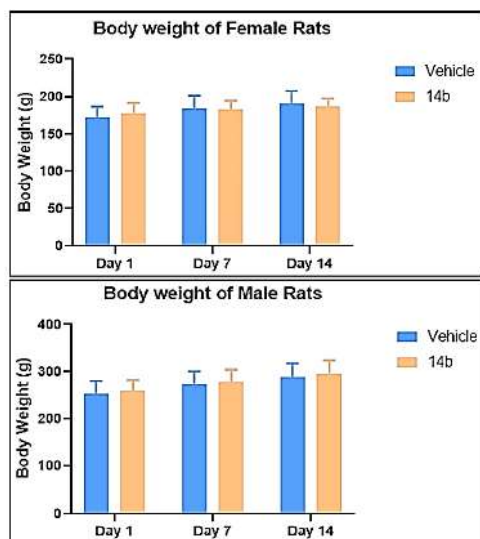| Parameter | Male rats | | Female rats | |
|---|---|---|---|---|
| | Vehicle[a] | 14b[a] | Vehicle[a] | 14b[a] |
| WBC ($10^3/\mu$L) | 6.11 ± 1.83 | 6.52 ± 0.56 | 4.48 ± 1.17 | 6.16 ± 1.35 |
| RBC ($10^6/\mu$L) | 8.11 ± 0.37 | 8.05 ± 0.46 | 6.99 ± 0.64 | 7.32 ± 0.14 |
| HGB (g/dL) | 14.5 ± 0.6 | 14.8 ± 0.5 | 12.7 ± 1.4 | 13.7 ± 0.2 |
| HCT (%) | 47.5 ± 2.0 | 47.6 ± 1.5 | 41.8 ± 4.1 | 43.8 ± 0.7 |
| MCHC (g/dL) | 30.58 ± 0.15 | 31.08 ± 0.34 | 30.28 ± 0.47 | 31.2 ± 0.1 |
| PLT ($10^3/\mu$L) | 638 ± 64 | 783 ± 58 | 504 ± 168 | 825 ± 81 |
| NEUT ($10^3/\mu$L) | 0.763 ± 0.213 | 1.112 ± 0.196 | 0.725 ± 0.212 | 1.130 ± 0.247 |
| LYMPH ($10^3/\mu$L) | 4.75 ± 1.57 | 4.90 ± 0.35 | 3.31 ± 0.85 | 4.45 ± 1.13 |
| MONO ($10^3/\mu$L) | 0.371 ± 0.152 | 0.251 ± 0.112 | 0.314 ± 0.118 | 0.332 ± 0.115 |
| EOSIN ($10^3/\mu$L) | 0.053 ± 0.023 | 0.080 ± 0.020 | 0.059 ± 0.026 | 0.126 ± 0.068 |
| BASO ($10^3/\mu$L) | 0.173 ± 0.067 | 0.172 ± 0.59 | 0.071 ± 0.037 | 0.123 ± 0.064 |

[a] Values expressed as mean ± SD; $n = 5$, Male and female Wister rats, vehicle = Tween-80 + 0.5 % Methyl Cellulose (1:99), administered through oral gavage route.

lines and dose linearity in rat and mice were conducted for **ZYBT1** and reported earlier [35]. Overall pre-clinical profile of **ZYBT1** indicates that the new class BTK inhibitor could be viable therapeutic option for the treatment of autoimmune diseases like cancer and RA.

## 5. Experimental section

### 5.1. Chemistry

All the solvents and reagents were purchase from commercial sources and were used without further purification or were prepared

**Table 8**
Serum chemistry parameter after two weeks treatment of 14b (100 mg/kg/day).

| Parameter | Male rats | | Female rats | |
|---|---|---|---|---|
| | Vehicle[a] | 14b[a] | Vehicle[a] | 14b[a] |
| GLU (mg/dL) | 108.16 ± 19.74 | 82.46 ± 9.88 | 85.54 ± 15.27 | 102.48 ± 11.14 |
| TRI (mg/dL) | 177.08 ± 58.29 | 145.22 ± 39.75 | 68.94 ± 20.30 | 56.56 ± 17.03 |
| TCHOL (mg/dL) | 69.70 ± 13.01 | 77.60 ± 10.84 | 60.80 ± 11.65 | 52.88 ± 6.97 |
| AST (U/L) | 92.62 ± 24.13 | 86.18 ± 5.52 | 102.82 ± 53.82 | 93.60 ± 22.63 |
| ALT (U/L) | 33.52 ± 6.69 | 38.26 ± 6.18 | 42.84 ± 10.11 | 40.54 ± 8.24 |
| ALP (U/L) | 106.98 ± 35.57 | 110.14 ± 14.51 | 56.76 ± 8.09 | 41.02 ± 9.16 |
| TBIL (mg/dL) | 0.09 ± 0.02 | 0.07 ± 0.02 | 0.10 ± 0.02 | 0.10 ± 0.01 |
| TP (g/dL) | 6.16 ± 0.23 | 6.32 ± 0.22 | 6.78 ± 0.28 | 6.60 ± 0.37 |
| ALB (g/dL) | 4.46 ± 0.24 | 4.40 ± 0.12 | 4.92 ± 0.22 | 5.10 ± 0.33 |
| GLB (g/dL) | 1.70 ± 0.10 | 1.92 ± 0.13 | 1.86 ± 0.15 | 1.50 ± 0.12 |
| CREAT (mg/dL) | 0.40 ± 0.04 | 0.41 ± 0.03 | 0.55 ± 0.04 | 0.49 ± 0.05 |
| UREA (mg/dL) | 33.40 ± 3.11 | 42.60 ± 6.70 | 48.78 ± 4.46 | 49.60 ± 7.30 |
| Ca (mg/dL) | 10.66 ± 0.27 | 11.06 ± 0.24 | 10.73 ± 0.27 | 11.00 ± 0.19 |
| PHOS (mg/dL) | 6.40 ± 0.48 | 6.50 ± 0.58 | 5.64 ± 0.31 | 5.82 ± 0.54 |
| Na$^+$ (mmol/L) | 143.80 ± 0.84 | 146.00 ± 1.22 | 144.60 ± 0.89 | 145.80 ± 0.84 |
| K$^+$ (mmol/L) | 4.61 ± 0.24 | 4.00 ± 0.23 | 4.70 ± 0.12 | 3.97 ± 0.27 |
| Cl$^-$ (mmol/L) | 99.88 ± 1.17 | 101.14 ± 0.71 | 102.56 ± 0.96 | 103.42 ± 1.39 |

[a] Values expressed as mean ± SD: $n = 5$, Male and female Wister rats, vehicle = Tween-80 + 0.5 % Methyl Cellulose (1:99), administered through oral gavage route.

according to published procedures. Reactions were monitored using thin layer silica gel chromatography (TLC) using 0.25 mm silica gel 60F plates from Merck. Plates were visualized by ultraviolet irradiation at 254 nm or/and staining with Ninhydrin and potassium permanganate. Products were purified by flash chromatography on combiflash instrument using pre packed redisep® column. The melting points were recorded on a scientific melting point apparatus and are uncorrected. NMR spectra were recorded at 400 MHz for $^1$H and 100 MHz for $^{13}$C on a 400 UltraSheild spectrometer (Bruker, Germany). Spectra were taken in indicated solvent at ambient temperature. Chemical shifts ($\delta$) are given in parts per million (ppm) with tetramethylsilane as an internal standard. Multiplicities are recorded as follows: s = singlet, d = doublet, dd = doublet of doublets, t = triplet, q = quartet, bs = broad singlet, m = multiplet. Coupling constants are reported as a $J$ values in Hertz (Hz). The purities of all final compounds were determined to be above 95 % by ultra-performance liquid chromatography (UPLC). UPLC conditions were as follows: YMC-Triart C18 column at room temperature, 100 × 2.0 mm, 1.9 µm, Mobile phase: 0.05 % TFA in Water: ACN (Gradient), 12 min. run; flow rate, 0.4 mL/min; UV detection $\lambda = 220$ nm. Mass spectra were recorded on Perkin-Elmer Sciex API 3000. ESI-Q-TOF-MS measurements were performed on a Xevo G2 QToF (waters, USA) mass spectrometer. HRMS was recorded on Brucker-Daltonics, Micro-TOF-Q II mass spectrometer.

### 5.2. Chemical synthesis

#### 5.2.1. 3-Amino-1H-pyrazole-4-carbonitrile (2)

Commercially available 2-(ethoxymethylene) malononitrile (50 g, 409 mmol) was added portion wise to Hydrazine monohydrate (32.2 mL, 655 mmol), at 25 °C. Reaction mixture was refluxed for 3 h. Reaction mixture was cooled at room temperature and concentrated under reduced pressure. The resulting solid was suspended in cold water (50 mL), stirred for 30 min. and refrigerated at 4 °C, overnight. Solid product thus obtained was filtered and washed with cold water (2 × 30 mL).
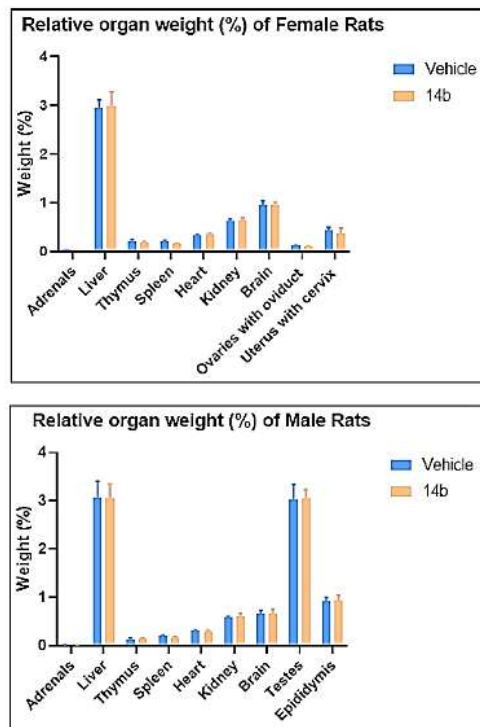
Fig. 6. Relative organ weights (%) after two weeks treatment of 14b (100 mg/kg/day).Values expressed as mean: $n = 5$, Male and female Wister rats, vehicle = Tween-80 + 0.5 % Methyl Cellulose (1:99), administered through oral gavage route.

Product was dried in an oven, at 50 °C for 4 h. 3-amino-1H-pyrazole-4-carbonitrile (30.5 g, 282 mmol, 69 % yield) was obtained as a light yellow orange solid. $^1$H NMR (400 MHz, DMSO-$d_6$) δ ppm 6.18 (bs, 2H), 7.67 (s, 1H), 12.04 (s, 1H).

#### 5.2.2. 1H-Pyrazolo[3,4-d]pyrimidin-4-ylamine (3)

5-amino-1H-pyrazole-4-carbonitrile (26.5 g, 245 mmol) was added to formamide (78 mL, 1961 mmol), at 25 °C. Reaction mixture was refluxed at 180 °C, for 6 h. The reaction mixture was cooled to room temperature, added water (200 mL) and stirred for 1 h. Solid product was filtered *in vacuo* and washed with water (2 × 100 mL). Solid product was dried and suspended in ethanol (90 mL), stirred for 30 min and filtered, dried *in vacuo* to afford 1H-pyrazolo[3,4-d]pyrimidin-4-amine (28.7 g, 212 mmol, 87 % yield) as light yellow solid. $^1$H NMR (400 MHz, DMSO-$d_6$) δ ppm 7.66 (bs, 2H), 8.06 (s, 1H), 8.10 (s, 1H), 13.30 (s, 1H). ESI-MS: $m/z$ Calcd for $C_5H_5N_5$ 136.05 [M + H]$^+$, found 135.65.

#### 5.2.3. 3-Iodo-1H-pyrazolo[3,4-d]pyrimidin-4-ylamine (4)

To a stirred solution of 1H-pyrazolo[3,4-d]pyrimidin-4-amine (33.2 g, 246 mmol), in DMF (140 mL) was added N-iodosuccinamide (66.3 g, 295 mmol), at room temperature. Resulting slurry was heated at 85–90 °C, for 18 h. The reaction mixture was cooled to room temperature and added water (1 l), stirred for 20 min followed by addition of aqueous sodium thiosulfate solution (10 % w/v, 250 mL). Mixture was stirred for 30 min., filtered and washed with water (2 × 200 mL). Solid

product thus obtained was washed with cold Ethanol (2 × 100 mL), dried *in vacuo* at 60 °C, for 4 h to afford 3-iodo-1H-pyrazolo[3,4-d]pyrimidin-4-amine (54.4 g, 208 mmol, 85 % yield) as yellow solid product. $^1$H NMR (400 MHz, DMSO-$d_6$) δ ppm 8.14 (s, 1H), 13.78 (s, 1H). ESI-MS: $m/z$ Calcd for $C_5H_4IN_5$ 261.95 [M + H]$^+$, found 261.65.

#### 5.2.4. 3-(4-Phenoxy-phenyl)-1H-pyrazolo[3,4-d]pyrimidin-4-ylamine (5)

3-iodo-1H-pyrazolo[3,4-d]pyrimidin-4-amine (2.7 g, 10.34 mmol) was dissolved in dry DMF (67.5 mL), (4-phenoxyphenyl)boronic acid (3.32 g, 15.52 mmol), PdCl$_2$(PPh$_3$)$_2$ (0.726 g, 1.03 mmol) and aqueous KHCO$_3$ solution (25.9 mL, 51.17 mmol) was added. The reaction mixture purged with nitrogen, for 10 min. The reaction mixture was heated at 90 °C, for 3 h, under nitrogen atmosphere. Mixture was cooled to room temperature, filtered, diluted with cold water (350 mL) and stirred. Solid precipitated was filtered, washed with water (25 mL), and dried *in vacuo* to obtained crude product. The crude product was purified by flash column chromatography, using 0–5 % methanol in dichloromethane as a mobile phase to get pure 3-(4-Phenoxy-phenyl)-1H-pyrazolo[3,4-d]pyrimidin-4-ylamine (5), as off white solid (2.32 g, 7.65 mmol, 74 % Yield). $^1$H NMR (400 MHz, DMSO-$d_6$) δ ppm 7.07–7.10 (m, 2H), 7.16–7.20 (s, 3H), 7.40–7.46 (m, 2H), 7.63–7.70 (m, 2H), 8.24 (s, 1H). ESI-MS: $m/z$ Calcd for $C_{17}H_{13}N_5O$ 304.11 [M + H]$^+$, found 303.75.

#### 5.2.5. General procedure for the synthesis of compound 7a-h

To solution of various substituted alcohol 6a-h (1 mmol), in dry THF (10 mL) were added triphenyl phosphine (0.525 g, 2 mmol) and 3-(4-Phenoxy-phenyl)-1H-pyrazolo[3,4-d]pyrimidin-4-ylamine (0.303 g, 1 mmol). The reaction mixture was stirred for 15 min., cooled at 0 °C, and diisopropyl diazodicarboxylate (0.389 mL, 2 mmol) was added. Mixture was stirred at room temperature overnight. The reaction mixture was diluted with water, extracted with ethyl acetate (3 × 50 mL), organic layer was washed with water (50 mL) and brine (50 mL), dried over Na$_2$SO$_4$ and concentrated *in vacuo*. The crude product was purified by flash column chromatography, using 0–5 % methanol in dichloromethane to afford desired product 7a-h.

#### 5.2.6. General procedure for the synthesis of compound 8a-h

To stirred solution of 7a-h (0.5 mmol), in DCM (5 mL), cooled at 0 °C, TFA (0.564 mL, 7.32 mmol) was added dropwise. The reaction mixture was stirred at room temperature for 3 h and concentrated *in vacuo*. Mixture was diluted with water (10 mL), basified with saturated sodium bicarbonate (pH 8), an aqueous layer was extracted with dichloromethane (3 × 10 mL), washed with brine (15 mL), dried over Na$_2$SO$_4$, concentrated and dried *in vacuo*. The obtained compound 8a-h were used in the next step, without further purification.

#### 5.2.7. General procedure for the synthesis of compound 9a-h

To the solution of 8a-h (0.485 mmol), in dichloromethane (10 mL) was added triethyl amine (0.203 mL, 1.45 mmol) and cooled at 0 °C. Acrolyl chloride (0.05 g, 0.558 mmol) was added dropwise and stirred for 2 h. The reaction mixture was diluted with water (10 mL). Organic layer was separated and washed with brine (10 mL), dried over Na$_2$SO$_4$, concentrated and dried *in vacuo*. The obtained crude product was purified by preparative HPLC to get desired products 9a-h.

##### 5.2.7.1. 1-((3R,3'R)-3-(4-amino-3-(4-phenoxyphenyl)-1H-pyrazolo[3,4-d]pyrimidin-1-yl)-[1,3'-bipyrrolidin]-1'-yl)prop-2-en-1-one (9a). White solid; 48 % isolated yield; Purity 98.35 %; m.p = 175–177 °C; $^1$H NMR (400 MHz, DMSO-$d_6$) δ ppm 1.68–1.91 (m, 1H), 1.98–2.09 (m, 1H), 2.29–2.32 (m, 2H), 2.78–2.87 (m, 4H), 3.20–3.28 (m, 1H), 3.35–3.37 (m, 1H), 3.50–3.78 (m, 3H), 5.39–3.41 (m, 1H), 5.63–5.66 (m, 1H), 6.12–6.14 (m, 1H), 6.55–6.57 (m, 1H), 7.10–7.16 (m, 5H), 7.40–7.44 (m, 2H), 7.66 (d, $J$ = 8.4 Hz, 2H), 8.24 (s, 1H). $^{13}$C NMR (100 MHz, DMSO-$d6$) δ ppm 24.32, 34.21, 51.93, 52.81, 52.95, 55.68, 61.22, 63.25, 97.85, 119.43, 119.45, 124.25, 127.74, 127.97, 128.40, 128.82,

      

130.55, 130.59, 143.80, 154.42, 156.14, 156.78, 157.58, 158.67, 165.02; HRMS (ESI): calcd for $C_{28}H_{30}N_7O_2$, 496.2461; found 496.2463.

### 5.2.7.2. 1-((3S,3'R)-3-(4-amino-3-(4-phenoxyphenyl)-1H-pyrazolo[3,4-d]pyrimidin-1-yl)-[1,3'-bipyrrolidin]-1'-yl)prop-2-en-1-one (9b).

White solid; 45 % isolated yield; Purity 99.01 %; m.p = 171–173 °C; $^1$H NMR (400 MHz, DMSO-$d_6$) δ ppm 1.71–1.90 (m, 1H), 1.98–2.12 (m, 1H), 2.29–2.32 (m, 2H), 2.78–2.90 (m, 4H), 3.17–3.26 (m, 1H), 3.35–3.38 (m, 1H), 3.50–3.78 (m, 3H), 5.39–3.41 (m, 1H), 5.64–5.65 (m, 1H), 6.08–6.13 (m,1H), 6.65–6.60(m, 1H), 7.10–7.19 (m, 5H), 7.41–7.44 (m, 2H), 7.66 (d, J = 8.0 Hz, 2H), 8.24 (s, 1H). $^{13}$C NMR (100 MHz, DMSO-$d_6$) δ ppm 24.33, 34.21, 51.95, 52.83, 52.95, 55.68, 61.25, 63.24, 97.85, 119.41, 119.43, 124.25, 127.74, 127.96, 128.40, 128.82, 130.51, 130.55, 143.80, 154.42, 156.15, 156.80, 157.58, 158.67, 165.03; HRMS (ESI): calcd for $C_{28}H_{30}N_7O_2$, 496.2461; found 496.2458.

### 5.2.7.3. (R)-1-(4-(3-(4-amino-3-(4-phenoxyphenyl)-1H-pyrazolo[3,4-d]pyrimidin-1-yl)pyrrolidin-1-yl)piperidin-1-yl)prop-2-en-1-one (9c).

White solid; 56 % isolated yield; Purity 99.14 %; m.p = 165–167 °C; $^1$H NMR (400 MHz, DMSO-$d_6$) δ ppm 1.27–1.31 (m, 4H), 1.39–1.71 (m, 1H),1.86–1.97 (m, 1H), 2.29–2.32 (m, 2H), 2.80–2.89 (m, 3H),3.10–3.25 (m, 2H), 3.89–4.01 (m, 1H), 4.12–4.18 (m, 1H), 5.39–3.41 (m, 1H), 5.62–5.65 (m, 1H), 6.05 (dd, J = 16.4, 2.4 Hz, 1H), 6.73–6.80 (m, 1H), 7.10–7.20 (m, 5H), 7.41–7.45 (m, 2H), 7.66 (d, J = 8.8 Hz, 2H), 8.24 (s, 1H). $^{13}$C NMR (100 MHz, DMSO-$d_6$) δ ppm 24.30, 28.22, 28.23, 38.81, 48.57, 49.00, 54.20, 63.25, 97.88, 119.41, 119.45, 124.25, 127.73, 127.97, 128.38, 128.80, 130.56, 130.60, 143.83, 154.42, 156.14, 156.79, 157.58, 158.65, 165.00; HRMS (ESI): calcd for $C_{29}H_{32}N_7O_2$, 510.2617; found 510.2623.

### 5.2.7.4. 1-(5-(2-(4-amino-3-(4-phenoxyphenyl)-1H-pyrazolo[3,4-d]pyrimidin-1-yl)ethyl)hexahydropyrrolo[3,4-c]pyrrol-2(1H)-yl)prop-2-en-1-one (9d).

White solid; 56 % isolated yield; Purity 98.83 %; m.p = 148–150 °C; $^1$H NMR (400 MHz, CDCl₃) δ ppm 2.57–2.70 (m, 4H), 2.75–2.77 (m, 1H), 2.85–2.87 (m, 1H), 2.93–2.96 (m, 1H), 3.05–3.08 (m, 1H), 3.24–3.36 (m, 2H), 3.68–3.79 (m, 4H), 4.50–4.57 (m, 2H), 5.41 (bs, 2H), 5.62 (dd, J = 8.8, 3.2 Hz, 1H), 6.27–6.37 (m, 2H), 7.07–7.09 (m, 2H), 7.13–7.18 (m, 3H), 7.39 (t, J = 8.0 Hz, 2H), 7.66 (d, J = 6.4 Hz, 2H), 8.37 (s, 1H). $^{13}$C NMR (100 MHz, DMSO-$d6$) δ ppm 38.25, 51.69, 51.70, 52.47, 53.06, 58.23, 97.85, 119.43, 119.46, 124.23, 127.79, 127.97, 128.43, 128.86, 130.50, 130.54, 142.73, 154.28, 155.94, 156.82, 158.02, 158.12, 164.95; HRMS (ESI): calcd for $C_{28}H_{30}N_7O_2$, 496.2461; found 496.2468.

### 5.2.7.5. 1-(5-(4-amino-3-(4-phenoxyphenyl)-1H-pyrazolo[3,4-d]pyrimidin-1-yl)hexahydrocyclopenta[c]pyrrol-2(1H)-yl)prop-2-en-1-one (9e).

White solid; 67 % isolated yield; Purity 99.52 %; m.p = 170–172 °C; $^1$H NMR (400 MHz, CDCl₃) δ ppm 2.11–2.17 (m, 2H), 2.50–2.58 (m, 2H), 3.10–3.21 (m, 2H), 3.45–3.54 (m, 2H), 3.82–3.87 (m, 2H), 5.53–5.59 (m, 3H), 5.62 (dd, J = 9.6, 2.8 Hz, 1H), 6.36–6.50 (m, 2H), 7.07–7.09 (m, 2H), 7.13–7.20 (m, 3H), 7.37–7.41 (m, 2H), 7.62–7.66 (m, 2H), 8.36 (s, 1H). $^{13}$C NMR (100 MHz, DMSO-$d6$) δ ppm 37.95, 38.19, 42.53, 51.58, 52.08, 59.05, 97.91, 119.24, 119.26, 124.25, 127.69, 127.92, 128.38, 128.79, 130.56, 130.60, 143.80, 154.42, 156.14, 156.78, 157.59, 158.67, 165.03; HRMS (ESI): calcd for $C_{27}H_{27}N_6O_2$, 467.2195; found 467.2189.

### 5.2.7.6. 1-(6-(4-amino-3-(4-phenoxyphenyl)-1H-pyrazolo[3,4-d]pyrimidin-1-yl)-3-azabicyclo[3.2.0]heptan-3-yl)prop-2-en-1-one (9f).

White solid; 34 % isolated yield; Purity 98.54 %; m.p = 143–145 °C; $^1$H NMR (400 MHz, CDCl₃) δ ppm 2.08–2.11 (m, 1H), 2.45–2.48 (m, 1H), 3.35–3.50 (m, 2H), 3.73–3.77 (m, 1H), 3.86–3.89 (m, 1H), 4.21–4.27 (m, 1H), 4.42–4.46 (m, 1H), 5.51 (bs, 2H), 5.58 (m, 1H), 5.64 (dd, J = 10.0, 2.0 Hz, 1H), 6.36–6.50 (m, 2H), 7.08–7.19 (m, 5H), 7.38–7.41 (m, 2H), 7.62–7.66 (m, 2H), 8.36 (s, 1H). $^{13}$C NMR (100 MHz, DMSO-$d6$)

ppm 29.58, 33.64, 38.43, 52.11, 53.46, 59.65, 97.68, 119.61, 119.62, 123.86, 127.72, 127.89, 128.40, 128.82, 130.55, 130.59, 144.15, 154.42, 156.39, 156.81, 157.55, 158.64, 165.04; HRMS (ESI): calcd for $C_{26}H_{25}N_6O_2$, 453.2039; found 453.2045.

### 5.2.7.7. 1-(6-(4-amino-3-(4-phenoxyphenyl)-1H-pyrazolo[3,4-d]pyrimidin-1-yl)octahydro-2H-cyclopenta[c]pyridin-2-yl)prop-2-en-1-one (9g).

White solid; 63 % isolated yield; Purity 98.70 %; m.p = 158–160 °C; $^1$H NMR (400 MHz, CDCl₃) δ ppm 1.59–1.62 (m, 1H),1.79–1.83 (m, 1H), 2.10–2.43 (m, 4H), 2.58–2.60 (m, 1H), 2.73–2.74 (m, 1H), 3.16–3.35 (m, 1H), 3.59–4.13 (m, 3H), 5.47 (bs, 2H), 5.56–5.58 (m, 1H), 5.66–5.72 (m, 1H), 5.32 (dd, J = 16, 4.8 Hz, 1H), 6.53–6.63 (m, 1H), 7.08–7.10 (m, 2H), 7.13–7.20 (m, 3H), 7.38–7.42 (m, 2H), 7.67 (d, J = 8.4 Hz, 1H),8.39 (s, 1H). $^{13}$C NMR (100 MHz, DMSO-$d6$) δ ppm 26.92, 37.92, 38.15, 42.58, 42.63, 44.82, 45.73, 58.15, 97.85, 119.42, 119.44, 124.25, 127.68, 127.88, 128.40, 128.83, 130.56, 130.60, 143.77, 154.44, 156.11, 156.64, 157.58, 158.67, 165.03; HRMS (ESI): calcd for $C_{28}H_{29}N_6O_2$, 481.2352; found 481.2355.

### 5.2.7.8. 1-((7S,8aS)-7-(4-amino-3-(4-phenoxyphenyl)-1H-pyrazolo[3,4-d]pyrimidin-1-yl)hexahydropyrrolo[1,2-a]pyrazin-2(1H)-yl)prop-2-en-1-one (9h).

Light yellow solid; 60 % isolated yield; Purity 98.42 %; m.p = 162–164 °C; $^1$H NMR (400 MHz, CDCl₃) δ ppm 2.26–2.42 (m, 4H), 2.77–3.03 (m, 2H), 3.08–3.10 (m, 1H), 3.19–3.41 (m, 1H), 3.52–3.54 (m, 1H), 3.91–4.09 (m, 1H), 4.63–4.85 (m, 1H), 5.48–55 (m, 3H), 5.72 (d, J = 10.4 Hz, 1H), 5.72 (d, J = 16.8 Hz, 1H), 5.32 (dd, J = 16.4, 10 Hz, 1H), 6.53–6.63 (m, 1H), 7.08–7.10 (m, 2H), 7.13–7.20 (m, 3H), 7.38–7.42 (m, 2H), 7.67 (d, J = 8.4 Hz, 1H), 8.39 (s, 1H). $^{13}$C NMR (100 MHz, DMSO-$d6$) δ ppm 26.85, 42.28, 43.36, 45.66, 48.12, 59.21, 60.18, 97.86, 119.41, 119.43, 124.21, 127.66, 127.89, 128.38, 128.81, 130.53, 130.58, 143.80, 154.42, 156.15, 156.82, 157.54, 158.64, 165.01; HRMS (ESI): calcd for $C_{27}H_{28}N_7O_2$, 482.2304; found 482.2311.

### 5.2.8. Tert-butyl-5-(4-amino-3-iodo-1H-pyrazolo[3,4-d]pyrimidin-1-yl) hexahydrocyclopenta[c] pyrrole-2(1H)-carboxylate (10)

3-iodo-1H-pyrazolo[3,4-d]pyrimidin-4-amine (2 g, 7.66 mmol) was dissolved in dry THF (50 mL), tert-butyl 5-hydroxyhexahydrocyclopenta[c]pyrrole-2(1H)-carboxylate (1.72 g 7.66 mmol) and triphenylphosphine (4.02 g, 15.32 mmol) were added in it, stirred for 15 min., the reaction mixture cooled at 0 °C and diisopropyl diazodicarboxylate (2.98 mL, 15.32 mmol) was added. The reaction mixture was stirred at room temperature overnight. Mixture was diluted with water (50 mL), extracted with ethyl acetate (2 × 50 mL), organic layer was washed with water (50 mL) and brine (50 mL), dried over Na₂SO₄, concentrated and dried *in vacuo*. The crude product was purified by flash column chromatography using 0–5 % methanol in dichloromethane to afford tert-butyl-5-(4-amino-3-iodo-1H-pyrazolo[3,4-d]pyrimidin-1-yl)hexahydrocyclopenta[c]pyrrole-2(1H)-carboxylate as white solid (2.4 g, 5.10 mmol, 66 % yield)).

### 5.2.9. General procedure for the synthesis of compounds 12a-p

Tert-butyl 5-(4-amino-3-iodo-1H-pyrazolo[3,4-d]pyrimidin-1-yl) hexahydrocyclopenta[c]pyrrole-2(1H)-carboxylate (0.4 g, 0.85 mmol) was dissolved in dry DMF (10 mL), substituted boronic acid **11a-p** (0.85 mmol), PdCl₂(PPh₃)₂ (60 mg, 0.085 mmol) and aqueous KHCO₃ solution (2.55 mL, 5.10 mmol) was added and the reaction mixture was purged with nitrogen, for 10 min. The reaction mixture was heated at 90 °C for 3 h, under nitrogen atmosphere. Mixture was cooled to room temperature, filtered through Celite, diluted with cold water (50 mL) and extracted with ethyl acetate (3 × 20 mL). Combined organic layer was washed with water (20 mL) and brine (20 mL), dried over Na₂SO₄, concentrated and dried *in vacuo*. The crude product was purified by flash column chromatography, using 0–5 % methanol in dichloromethane as a mobile phase to afford desired product 12a-p.

13

### 5.2.10. General procedure for the synthesis of compound 13a-p

Refer to general procedure for the synthesis of 13a-p, as described in section 5.2.6.

### 5.2.11. General procedure for the synthesis of compound 14a-p

Refer to general procedure for the synthesis of 14a-p, as described in section 5.2.7.

#### 5.2.11.1. 4-(1-(2-acryloyloctahydrocyclopenta[c]pyrrol-5-yl)-4-amino-1H-pyrazolo[3,4-d]pyrimidin-3-yl)-N-(pyrazin-2-yl)benzamide(14a).

White solid; 58 % isolated yield; Purity 99.16 %; m.p > 220 °C; $^1$H NMR (400 MHz, DMSO-$d_6$) δ ppm 2.06–2.09 (m, 2H), 2.31–2.39 (m, 2H), 3.07–3.11 (m, 2H), 3.34–3.39 (m, 1H), 3.53–3.54 (m, 1H), 3.61–3.64 (m, 1H), 3.76–3.79 (m, 1H), 5.43–5.46 (m, 1H), 5.67 (dd, $J$ = 10, 2.4 Hz, 1H), 6.14 (dd, $J$ = 16.8, 2.8 Hz, 1H), 6.62 (dd, $J$ = 16.8, 10.4 Hz, 1H), 7.82 (d, $J$ = 8.4 Hz, 2H), 8.22 (d, $J$ = 8.4 Hz, 2H), 8.26 (s, 1H), 8.44 (d, $J$ = 2.4 Hz, 1H), 8.49–8.50 (m, 1H), 9.45 (d, $J$ = 1.6 Hz, 1H), 11.22 (s, 1H). $^{13}$C NMR (100 MHz, DMSO-d6) δ ppm 37.96, 38.19, 42.52, 51.56, 52.09, 58.10, 97.58, 127.23, 128.58, 129.04, 129.35, 129.69, 130.05, 134.53, 135.46, 136.82, 137.32, 139.66, 145.39, 147.33, 151.07, 152.34, 154.09, 163.87, 166.17; HRMS (ESI): calcd for $C_{26}H_{26}N_9O_2$, 496.2209; found 496.2213.

#### 5.2.11.2. 4-(1-(2-acryloyloctahydrocyclopenta[c]pyrrol-5-yl)-4-amino-1H-pyrazolo[3,4-d]pyrimidin-3-yl)-N-(pyridin-3-yl)benzamide (14b).

White solid; 71 % isolated yield; Purity 99.72 %; m.p > 220 °C; $^1$H NMR (400 MHz, DMSO-$d_6$) δ ppm 1.99–2.05 (m, 2H), 2.35–2.38 (m, 2H), 3.00–3.07 (m, 2H), 3.35–3.39 (m, 1H), 3.51–3.54 (m, 1H), 3.61–3.66 (m, 1H), 3.76–3.81 (m, 1H), 5.42–5.46 (m, 1H), 5.67 (dd, $J$ = 10.4, 2.4 Hz, 1H), 6.14 (dd, $J$ = 16.8, 2.4 Hz, 1H), 6.62 (dd, $J$ = 16.8, 10.4 Hz, 1H), 7.17–7.12 (m, 1H), 7.79 (d, $J$ = 8.4 Hz, 2H), 7.84–7.88 (m, 1H), 8.20 (d, $J$ = 8.4 Hz, 2H), (8.21–8.23 (m, 1H), 8.26 (s, 1H), 8.40–8.41 (m, 1H), 10.87 (s, 1H). $^{13}$C NMR (100 MHz, DMSO-d6) δ ppm 37.95, 38.19, 42.53, 51.58, 52.08, 58.09, 97.58, 115.63, 120.60, 127.20, 128.83, 129.02, 129.48, 129.82, 130.05, 134.53, 135.46, 139.76, 145.39, 147.33, 152.01, 152.34, 154.09, 163.87, 166.17; HRMS (ESI): calcd for $C_{27}H_{27}N_8O_2$, 495.2257; found 495.2268.

#### 5.2.11.3. 4-(1-(2-acryloyloctahydrocyclopenta[c]pyrrol-5-yl)-4-amino-1H-pyrazolo[3,4-d]pyrimidin-3-yl)-N-(pyridin-3-yl)benzamide (14c).

White solid; 70 % isolated yield; Purity 99.34 %; m.p > 220 °C; $^1$H NMR (400 MHz, DMSO-$d_6$) δ ppm 2.05–2.08 (m, 2H), 2.31–2.37 (m, 2H), 2.98–3.08 (m, 2H), 3.35–3.39 (m, 1H), 3.51–3.55 (m, 1H), 3.61–3.66 (m, 1H), 3.77–3.79 (m, 1H), 5.43–5.45 (m, 1H), 5.67 (dd, $J$ = 10.4, 2.4 Hz, 1H), 6.14 (dd, $J$ = 16.8, 2.4 Hz, 1H), 6.62 (dd, $J$ = 16.4, 10.0 Hz, 1H), 7.40–7.43 (m, 1H), 7.84 (d, $J$ = 8.4 Hz, 2H), 8.16 (d, $J$ = 8.4 Hz, 2H), 8.21–8.23 (m, 1H), 8.26 (s, 1H), 8.32–8.33 (m, 1H), 8.96 (d, $J$ = 2.4 Hz, 1H), 10.54 (s, 1H). $^{13}$C NMR (100 MHz, DMSO-$d_6$) δ ppm 37.93, 38.18, 42.58, 51.56, 52.06, 58.10, 97.61, 120.68, 121.43, 127.28, 128.89, 129.08, 129.46, 129.80, 130.01, 134.53, 134.64, 135.51, 139.58, 140.21, 145.38, 147.31, 152.35, 154.08, 163.80, 166.16; HRMS (ESI): calcd for $C_{27}H_{27}N_8O_2$, 495.2257; found 495.2256.

#### 5.2.11.4. 4-(1-(2-acryloyloctahydrocyclopenta[c]pyrrol-5-yl)-4-amino-1H-pyrazolo[3,4-d]pyrimidin-3-yl)-N-(4-methylpyridin-2-yl)benzamide (14d).

White solid; 62 % isolated yield; Purity 98.73 %; m.p > 220 °C; $^1$H NMR (400 MHz, CDCl$_3$) δ ppm 2.09–2.20 (m, 2H), 2.43 (s, 3H), 2.54–2.59 (m, 2H), 3.12–3.23 (m, 2H), 3.46–3.56 (m, 2H), 3.83–3.86 (m, 2H), 5.44 (bs, 1H), 5.56–5.60 (m, 1H), 5.69 (dd, $J$ = 10.0, 2.4 Hz, 1H), 6.36 6.50 (m, 2H), 6.94 (d, $J$ = 5.2 Hz, 1H), 7.86 (d, $J$ = 8.0 Hz, 2H), 8.10 (d, $J$ = 8.4 Hz, 2H), 8.19 (d, $J$ = 5.2 Hz, 2H), 8.26 (s, 1H), 8.39 (s, 1H), 8.59 (bs, 1H). $^{13}$C NMR (100 MHz, DMSO-$d_6$) δ ppm 20.28, 37.95, 38.19, 42.54, 51.58, 52.07, 58.08, 97.56, 113.42, 120.73, 127.21, 128.76, 128.95, 129.43, 129.77, 130.04, 134.61, 135.47, 140.38, 145.31, 147.29, 152.35, 154.11, 158.22, 158.76, 163.83,

166.15; HRMS (ESI): calcd for $C_{28}H_{29}N_8O_2$, 509.2413; found 509.2410.

#### 5.2.11.5. 4-(1-(2-acryloyloctahydrocyclopenta[c]pyrrol-5-yl)-4-amino-1H-pyrazolo[3,4-d]pyrimidin-3-yl)-N-(4-(trifluoromethyl)pyridin-2-yl)benzamide (14e).

White solid; 65 % isolated yield; Purity 99.11 %; m.p > 220 °C; $^1$H NMR (400 MHz, CDCl$_3$) δ ppm 2.15–2.18 (m, 2H), 2.53–2.57 (m, 2H), 3.12–3.20 (m, 2H), 3.47–3.56 (m, 2H), 3.83–3.87 (m, 2H), 5.56–5.60 (m, 3H), 5.70 (dd, $J$ = 9.6, 2.4 Hz, 1H), 6.36–6.51 (m,2H), 7.34 (d, $J$ = 5.2 Hz, 1H), 7.88 (d, $J$ = 8.4 Hz, 2H), 8.14 (d, $J$ = 8.4 Hz, 2H), 8.39 (s, 1H), 8.51 (d, $J$ = 5.2 Hz, 1H), 8.73 (s, 1H), 9.02 (s, 1H). $^{13}$C NMR (100 MHz, DMSO-$d_6$) δ ppm 37.93, 38.20, 42.54, 51.58, 52.07, 58.08, 97.61, 114.16, 119.41, 123.93, 127.22, 128.85, 129.04, 129.17, 129.81, 130.02, 134.56, 135.40, 145.21, 147.19, 147.38, 149.67, 152.29, 154.12, 155.51 163.76, 166.20; HRMS (ESI): calcd for $C_{28}H_{26}F_3N_8O_2$, 563.2131; found 563.2135.

#### 5.2.11.6. N-(4-(1-(2-acryloyloctahydrocyclopenta[c]pyrrol-5-yl)-4-amino-1H-pyrazolo[3,4-d]pyrimidin-3-yl)phenyl)picolinamide (14f).

White solid; 75 % isolated yield; Purity 98.33 %; m.p > 220 °C; $^1$H NMR (400 MHz, DMSO-$d_6$) δ ppm 2.04–2.08 (m, 2H), 2.32–2.37 (m, 2H), 2.98–3.08 (m, 2H), 3.35–3.39 (m, 1H), 3.51–3.55 (m, 1H), 3.61–3.66 (m, 1H), 3.77–3.79 (m, 1H), 5.41–5.42 (m, 1H), 5.67 (dd, $J$ = 10.4, 2.4 Hz, 1H), 6.14 (dd, $J$ = 16.4, 2.4 Hz, 1H), 6.62 (dd, $J$ = 16.8, 10.0 Hz, 1H), 7.65–7.71 (m, 3H), 8.09–8.12 (m, 3H), 8.19 (d, $J$ = 8.0 Hz,1H), 8.23 (s, 1H), 8.77 (d, $J$ = 4.4 Hz, 1H), 10.12 (s, 1H). $^{13}$C NMR (100 MHz, DMSO-$d_6$) δ ppm 37.95, 38.17, 42.53, 51.60, 52.09, 58.10, 97.59, 118.56, 118.82, 120.31, 121.46, 127.19, 128.89, 129.08, 130.17, 134.41, 135.62, 139.19, 145.42, 147.34, 149.08, 151.79, 152.28, 154.04, 163.82, 166.14; HRMS (ESI): calcd for $C_{27}H_{27}N_8O_2$, 495.2257; found 495.2251.

#### 5.2.11.7. 5-(1-(2-acryloyloctahydrocyclopenta[c]pyrrol-5-yl)-4-amino-1H-pyrazolo[3,4-d]pyrimidin-3-yl)-N-(pyridin-2-yl)picolinamide (14g).

White solid; 65 % isolated yield; Purity 99.55 %; m.p > 220 °C; $^1$H NMR (400 MHz, DMSO-$d_6$) δ ppm 2.08–2.11 (m, 2H), 2.32–2.39 (m, 2H), 2.85–3.05 (m, 2H), 3.35–3.39 (m, 1H), 3.54–3.55 (m, 1H), 3.61–3.63 (m, 1H), 3.76–3.78 (m, 1H), 5.45–5.47 (m, 1H), 5.67 (dd, $J$ = 12.0, 2.0 Hz, 1H), 6.14 (dd, $J$ = 16.8, 2.0 Hz, 1H), 6.62 (dd, $J$ = 16.8, 10.4 Hz, 1H), 7.21–7.24 (m, 1H), 7.92–7.94 (m, 1H), 8.28–8.33 (m, 4H), 8.42 (d, $J$ = 4.4 Hz, 1H), 8.99 (s, 1H), 10.47 (s, 1H). $^{13}$C NMR (100 MHz, DMSO-$d_6$) δ ppm 37.92, 38.17, 42.52, 51.58, 52.07, 58.08, 97.93, 116.51, 121.34, 124.78, 127.23, 130.19, 134.23, 136.44, 139.66, 140.59, 145.58, 147.07, 148.87, 149.73, 152.18, 152.30, 154.34, 163.11, 166.18; HRMS (ESI): calcd for $C_{26}H_{26}N_9O_2$, 496.2209; found 496.2201.

#### 5.2.11.8. 5-(1-(2-acryloyloctahydrocyclopenta[c]pyrrol-5-yl)-4-amino-1H-pyrazolo[3,4-d]pyrimidin-3-yl)-N-phenylpicolinamide (14h).

White solid; 60 % isolated yield; Purity 98.93 %; m.p > 220 °C; $^1$H NMR (400 MHz, DMSO-$d_6$) δ ppm 2.06–2.09 (m, 2H), 2.33–2.41 (m, 2H), 2.99–3.11 (m, 2H), 3.35–3.39 (m, 1H), 3.51–3.55 (m, 1H), 3.61–3.66 (m, 1H), 3.76–3.81 (m, 1H), 5.44–5.47 (m, 1H), 5.67 (dd, $J$ = 10.4, 2.4 Hz, 1H), 6.14 (dd, $J$ = 16.8, 2.4 Hz, 1H), 6.63 (dd, $J$ = 16.8, 10.4 Hz, 1H), 7.11–7.17 (m, 1H), 7.38 (t, $J$ = 8.0 Hz, 2H), 7.95 (d, $J$ = 7.6 Hz, 2H), 8.29 (d, $J$ = 7.6 Hz, 2H), 8.96 (s, 1H), 10.75 (s, 1H). $^{13}$C NMR (100 MHz, DMSO-$d_6$) δ ppm 37.97, 38.21, 42.57, 51.59, 52.06, 58.07, 97.53, 123.82, 124.51, 124.57, 134.12, 127.17, 128.77, 128.85, 128.86, 130.08, 135.91, 137.51, 141.37, 145.27, 147.42, 149.74, 152.26, 154.09, 163.89, 166.15; HRMS (ESI): calcd for $C_{27}H_{27}N_8O_2$, 495.2257; found 495.2264.

#### 5.2.11.9. 1-(5-(4-amino-3-(4-(2-(ethylthio)ethoxy)phenyl)-1H-pyrazolo[3,4-d]pyrimidin-1-yl)hexahydrocyclopenta[c]pyrrol-2(1H)-yl)prop-2-en-1-one (14i).

Yellow solid; 55 % isolated yield; Purity 99.19 %; m.p = 128–130 °C; $^1$H NMR (400 MHz, DMSO-$d_6$) δ ppm 1.23 (t, 3H, $J$ = 7.6

Hz), 2.01–2.07 (m, 2H), 2.30–2.37 (m, 2H), 2.66 (q, 2H, $J = 7.6$ Hz), 2.93 (t, $J = 6.4$ Hz, 2H), 2.96–2.99 (m, 1H), 3.05–3.08 (m, 1H), 3.36–3.0.37 (m, 1H), 3.49–3.53 (m, 1H), 3.60–3.65 (m, 1H), 3.75–3.80 (m, 1H), 4.21 (t, 2H, $J = 6.4$ Hz), 5.38–5.41 (m, 1H), 5.68 (dd, $J = 10.4$, 2.4 Hz, 1H), 6.16 (dd, $J = 16.8$, 2.4 Hz, 1H), 6.65 (dd, $J = 16.8$, 10.4 Hz, 1H), 7.11 (d, $J = 8.8$ Hz, 2H), 7.59 (d, $J = 8.8$ Hz, 2H), 8.21 (s, 1H). $^{13}$C NMR (100 MHz, DMSO-$d_6$) δ ppm 14.28, 25.89, 33.82, 37.97, 38.21, 42.53, 51.56, 52.06, 58.08, 67.23, 97.91, 115.60, 126.07, 127.20, 130.05, 130.10, 143.75, 151.85, 154.14, 155.96, 158.62, 166.17; HRMS (ESI): calcd for $C_{25}H_{31}N_6O_2S$, 479.2229; found 479.2233.

*5.2.11.10.* 1-(5-(4-amino-3-(4-(2-(isopropylthio)ethoxy)phenyl)-1H-pyr-azolo[3,4-d]pyrimidin-1-yl)hexahydrocyclopenta[c]pyrrol-2(1H)-yl)prop-2-en-1-one (14j). White solid; 51 % isolated yield; Purity 98.24 %; m.p = 115–117 °C; $^1$H NMR (400 MHz, DMSO-$d_6$) δ ppm 1.24 (d, $J = 6.4$ Hz, 6H), 1.97–2.07 (m, 2H), 2.28–2.37 (m, 2H), 2.90–3.00 (m, 3H), 3.02–3.11 (m, 2H), 3.34–3.37 (m, 1H), 3.49–3.53 (m, 1H), 3.60–3.65 (m, 1H), 3.75–3.80 (m, 1H), 4.20 (t, $J = 6.4$ Hz, 2H), 5.37–5.41 (m, 1H), 5.68 (dd, $J = 10.4$, 2.8 Hz, 1H), 6.16 (dd, $J = 16.8$, 2.4 Hz, 1H), 6.65 (dd, $J = 16.8$, 10.4 Hz, 1H), 7.10 (d, $J = 8.8$ Hz, 2H), 7.59 (d, $J = 8.8$ Hz, 2H), 8.21 (s, 1H). $^{13}$C NMR (100 MHz, DMSO-$d_6$) δ ppm 24.46, 26.83, 37.95, 38.18, 42.56, 51.60, 52.09, 58.10, 66.49, 97.90, 115.55, 126.05, 127.19, 130.07, 130.11, 143.72, 151.83, 154.13, 155.96, 158.61, 166.17; HRMS (ESI): calcd for $C_{26}H_{33}N_6O_2S$, 493.2386; found 493.2383.

*5.2.11.11.* 1-(5-(4-amino-3-(4-(2-(ethylsulfonyl)ethoxy)phenyl)-1H-pyr-azolo[3,4-d]pyrimidin-1-yl)hexahydrocyclopenta[c]pyrrol-2(1H)-yl)prop-2-en-1-one (14k). White solid; 64 % isolated yield; Purity 98.70 %; m.p = 132–134 °C; $^1$H NMR (400 MHz, DMSO-$d_6$) δ ppm 1.29 (t, $J = 7.2$ Hz, 3H), 1.89–2.08 (m, 2H), 2.28–2.37 (m, 2H), 2.96–2.99 (m, 1H), 3.06–3.08 (m, 1H), 3.22 (q, $J = 7.2$ Hz, 2H), 3.36–3.37 (m, 1H), 3.49–3.53 (m, 1H), 3.60–3.65 (m, 3H), 3.75–3.80 (m, 1H), 4.43 (t, $J = 5.6$ Hz, 2H), 5.40–5.41 (m, 1H), 5.68 (dd, $J = 10.4$, 2.4 Hz, 1H), 6.16 (dd, $J = 16.8$, 2.0 Hz, 1H), 6.65 (dd, $J = 16.8$, 10.4 Hz, 1H), 7.16 (d, $J = 8.8$ Hz, 2H), 7.61 (d, $J = 8.4$ Hz, 2H), 8.22 (s, 1H). $^{13}$C NMR (100 MHz, DMSO-$d_6$) δ ppm 9.24, 37.96, 38.18, 42.45, 51.56, 51.91, 53.78, 58.22, 62.61, 63.19, 67.23, 98.09, 115.43, 125.84, 127.16, 129.81, 130.05, 142.57, 152.41, 154.04, 155.96, 158.62, 166.17; HRMS (ESI): calcd for $C_{25}H_{31}N_6O_4S$, 511.2127; found 511.2139.

*5.2.11.12.* 1-(5-(4-amino-3-(4-((2-ethoxyethyl)thio)phenyl)-1H-pyrazolo[3,4-d]pyrimidin-1-yl)hexahydrocyclopenta[c]pyrrol-2(1H)-yl)prop-2-en-1-one (14l). White solid; 49 % isolated yield; Purity 99.45 %; m.p = 111–113 °C; $^1$H NMR (400 MHz, DMSO-$d_6$) δ ppm 1.10 (t, $J = 6.8$ Hz, 3H), 2.02–2.07 (m, 2H), 2.30–2.35 (m, 2H), 2.96–2.99 (m, 1H), 3.05–3.09 (m, 1H), 3.20 (t, $J = 6.4$ Hz, 2H), 3.53–3.43 (m, 4H), 3.65–3.58 (m, 3H), 3.80–3.75 (m, 1H), 5.43–5.38 (m, 1H), 5.66 (dd, $J = 10.0$, 2.4 Hz, 1H), 6.14 (dd, $J = 16.4$, 2.4 Hz, 1H), 6.62 (dd, $J = 16.4$, 10.0 Hz, 1H), 7.48 (d, $J = 8.4$ Hz, 2H), 7.60 (d, $J = 8.4$ Hz, 2H), 8.22 (s, 1H). $^{13}$C NMR (100 MHz, DMSO-$d_6$) δ ppm 15.55, 32.18, 37.76, 38.18, 41.12, 41.59, 50.85, 53.77, 57.19, 65.90, 68.82, 74.92, 97.87, 127.22, 128.62, 129.24, 130.05, 130.60, 137.46, 143.44, 154.27, 156.00, 158.61, 166.18; HRMS (ESI): calcd for $C_{25}H_{31}N_6O_2S$, 479.2229; found 479.2234.

*5.2.11.13.* 1-(5-(4-amino-3-(4-((3-methoxypropyl)thio)phenyl)-1H-pyr-azolo[3,4-d]pyrimidin-1-yl)hexahydrocyclopenta[c]pyrrol-2(1H)-yl)prop-2-en-1-one (14m). Light pink solid; 58 % isolated yield; Purity 98.05 %; m.p = 105–107 °C; $^1$H NMR (400 MHz, DMSO-$d_6$) δ ppm. 1.83–1.86 (m, 2H), 2.03–2.07 (m, 2H), 2.30–2.35 (m, 2H), 2.96–2.99 (m, 1H), 3.08 (t, $J = 7.2$ Hz, 3H), 3.23 (s, 3H), 3.36–3.37 (m, 1H), 3.45 (t, $J = 6.0$ Hz, 2H), 3.52–3.53 (m, 1H), 3.60–3.62 (m, 1H), 3.75–3.78 (m, 1H), 5.37–5.40 (m, 1H), 5.68 (dd, $J = 10.4$, 2.4 Hz, 1H), 6.16 (dd, $J = 16.8$, 2.4 Hz, 1H), 6.65 (dd, $J = 16.8$, 10.0 Hz, 1H), 7.46 (d, $J = 8.4$ Hz, 2H), 7.61 (d, $J =$

8.4 Hz, 2H), 8.22 (s, 1H). $^{13}$C NMR (100 MHz, DMSO-$d_6$) δ ppm 27.12, 34.83, 37.91, 38.01, 42.53, 51.56, 52.06, 58.08, 59.11, 73.59, 97.87, 127.10, 127.86, 127.91, 130.10, 131.07, 134.15, 143.58, 151.85, 154.14, 155.96, 166.17; HRMS (ESI): calcd for $C_{25}H_{31}N_6O_2S$, 479.2229; found 479.2220.

*5.2.11.14.* 1-(5-(4-amino-3-(4-((3-(methylthio)propyl)thio)phenyl)-1H-pyrazolo[3,4-d]pyrimidin-1-yl)hexahydrocyclopenta[c]pyrrol-2(1H)-yl)prop-2-en-1-one (14n). White solid; 69 % isolated yield; Purity 99.38 %; m.p = 122–124 °C; $^1$H NMR (400 MHz, DMSO-$d_6$) δ ppm. 1.91 (m, 2H), 2.05–2.07 (m, 5H), 2.30–2.35 (m, 2H), 2.62 (t, $J = 7.2$ Hz, 2H), 2.96–2.98 (m, 1H), 3.06–3.08 (m, 1H), 3.13 (t, $J = 7.2$ Hz, 2H), 3.37–3.37 (m, 1H), 3.49–3.53 (m, 1H), 3.60–3.65 (m, 1H), 3.75–3.80 (m, 1H), 5.39–5.42 (m, 1H), 5.68 (dd, $J = 10.0$, 2.4 Hz, 1H), 6.16 (dd, $J = 16.8$, 2.4 Hz, 1H), 6.65 (dd, $J = 16.8$, 10.0 Hz, 1H), 7.48 (d, $J = 8.4$ Hz, 2H), 7.62 (d, $J = 8.4$ Hz, 2H), 8.22 (s, 1H). $^{13}$C NMR (100 MHz, DMSO-$d_6$) δ ppm 15.08, 26.94, 32.84, 33.26, 37.93, 38.11, 42.32, 58.19, 67.23, 97.87, 127.20, 128.73, 128.92, 129.38, 129.72, 130.09, 130.27, 135.58, 143.31, 154.24, 154.96, 158.47, 166.11; HRMS (ESI): calcd for $C_{25}H_{31}N_6OS_2$, 495.2001; found 495.1993.

*5.2.11.15.* 1-(5-(4-amino-3-(4-((2-(ethylthio)ethyl)thio)phenyl)-1H-pyr-azolo[3,4-d]pyrimidin-1-yl)hexahydrocyclopenta[c]pyrrol-2(1H)-yl)prop-2-en-1-one (14o). White solid; 55 % isolated yield; Purity 99.31 %; m.p = 131–133 °C; $^1$H NMR (400 MHz, DMSO-$d_6$) δ ppm. 1.17 (t, $J = 7.4$ Hz, 3H), 2.04–2.07 (m, 2H), 2.30–2.35 (m, 2H), 2.59 (q, $J = 7.4$ Hz, 2H), 2.74–2.78 (m, 2H), 2.96–3.01 (m, 1H), 3.04–3.08 (m, 1H), 3.22–3.26 (m, 2H), 3.34–3.38 (m, 1H), 3.51–3.53 (m, 1H), 3.59–3.63 (m, 1H), 3.75–3.79 (m, 1H), 5.38–5.43 (m, 1H), 5.66 (dd, $J = 10.4$, 2.4 Hz, 1H), 6.14 (dd, $J = 16.8$, 2.4 Hz, 1H), 6.62 (dd, $J = 16.8$, 10.4 Hz, 1H), 7.49 (d, $J = 8.0$ Hz, 2H), 7.61 (d, $J = 8.0$ Hz, 2H), 8.22 (s, 1H). $^{13}$C NMR (100 MHz, DMSO-$d_6$) δ ppm 14.73, 26.57, 34.09, 37.95, 38.14, 38.23, 41.86, 51.59, 52.22, 58.10, 98.03, 127.12, 128.55, 128.79, 129.06, 129.41, 129.68, 130.02, 135.53, 143.68, 154.14, 155.38, 158.28, 166.13; HRMS (ESI): calcd for $C_{25}H_{31}N_6OS_2$, 495.2001; found 495.2011.

*5.2.11.16.* 1-(5-(4-amino-3-(4-((2-(ethylsulfonyl)ethyl)thio)phenyl)-1H-pyrazolo[3,4-d]pyrimidin-1-yl)hexahydrocyclopenta[c]pyrrol-2(1H)-yl)prop-2-en-1-one (14p). White solid; 47 % isolated yield; Purity 98.26 %; m.p = 120–122 °C; $^1$H NMR (400 MHz, DMSO-$d_6$) δ ppm. 1.43 (t, $J = 7.6$ Hz, 3H), 2.19–2.13 (m, 2H), 2.58–2.53 (m, 2H), 3.06 (q, $J = 7.6$ Hz, 2H), 3.28–3.11 (m, 4H), 3.44–3.40 (m, 2H), 3.55–3.47 (m, 2H), 3.88–3.93 (m, 2H), 5.64–5.55 (m, 3H), 5.71 (dd, $J = 10.0$, 2.8 Hz, 1H), 6.38–6.51 (m, 2H), 7.54 (d, $J = 8.0$ Hz, 2H), 7.69 (d, $J = 8.4$ Hz, 2H), 8.41 (s, 1H). $^{13}$C NMR (100 MHz, DMSO-$d_6$) δ ppm 8.25, 26.37, 37.91, 38.08, 41.86, 49.74, 51.56, 52.18, 57.88, 58.12, 98.95, 127.16, 128.51, 128.76, 129.01, 129.35, 129.73, 130.05, 135.54, 143.63, 154.18, 155.33, 158.26, 166.14; HRMS (ESI): calcd for $C_{25}H_{31}N_6O_3S_2$, 527.1899; found 527.1903.

*5.2.12. General procedure for the synthesis of compounds 14q and 14s-u.*
To the solution of 13b (0.485 mmol), in DMF (10 mL) were added corresponding acids (0.533 mmol) and DIPEA (0.203 mL, 1.45 mmol) and cooled at 0 °C, followed by addition of HBTU (0.533 mmol). The reaction mixture was stirred for 18 h. Mixture was diluted with water (10 mL) and extracted with ethyl acetate (3 × 10 mL). Combined organic layer was washed with water (10 mL) and brine (10 mL), dried over Na$_2$SO$_4$ and concentrated *in vacuo*. The obtained crude product was purified by preparative HPLC to get the desired products 14q, 14s-u.

*5.2.12.1. 4-(4-amino-1-(2-(but-2-ynoyl)octahydrocyclopenta[c]pyrrol-5-yl)-1H-pyrazolo[3,4-d]pyrimidin-3-yl)-N-(pyridin-2-yl)benzamide (14q).* White solid; 70 % isolated yield; Purity 99.60 %; m.p > 220 °C; $^1$H NMR (400 MHz, DMSO-$d_6$) δ ppm 2.01 (s, 3H), 2.04–2.08 (m, 2H), 2.32–2.36 (m, 2H), 3.04–3.05 (m, 2H), 3.27–3.28 (m, 1H), 3.54–3.55 (m, 2H),

15

3.81–3.82 (m, 1H),5.42–5.44 (m, 1H), 7.17–7.20 (m, 1H), 7.79 (d, *J* = 8.4 Hz, 2H), 7.86–7.87 (m, 1H), 8.18–8.23 (m,3H), 8.26 (s, 1H), 8.40–8.41 (m, 1H), 10.87 (s, 1H). $^{13}$C NMR (100 MHz, DMSO-$d_6$) δ ppm 3.72, 37.78, 38.17, 41.14, 41.61, 50.85, 53.78, 57.36, 74.92, 88.03, 98.11, 115.24, 120.36, 128.60, 129.26, 134.24, 136.71, 138.61, 143.12, 148.43, 151.88, 152.62, 154.42, 156.09, 158.61, 166.04; HRMS (ESI): calcd for $C_{28}H_{27}N_8O_2$, 507.2257; found 507.2256.

*5.2.12.2. (E)-4-(4-amino-1-(2-(4-(dimethylamino)but-2-enoyl)octahy-drocyclopenta[c]pyrrol-5-yl)-1H-pyrazolo[3,4-d]pyrimidin-3-yl)-N-(pyr-idin-2-yl)benzamide (14s).* Light yellow solid; 41 % isolated yield; Purity 97.78 %; m.p = 195–197 °C; $^1$H NMR (400 MHz, MEOD) δ ppm 2.14–2.19 (m, 2H), 2.30 (s, 6H), 2.49–2.53(m, 2H), 3.14–3.28 (m, 4H), 3.53–3.54 (m, 1H), 3.62–3.62 (m, 1H), 3.76–3.80 (m, 1H), 3.89–3.92 (m, 1H), 5.54–5.55 (m, 1H), 6.52 (dd, *J* = 15.2, 1.2 Hz, 1H), 6.83–6.86 (m, 1H), 7.18–7.21 (m, 1H), 7.84–7.90 (m, 3H), 8.15–8.17 (m, 2H) 8.25–8.27 (m, 2H), 8.38–8.40 (m, 1H). $^{13}$C NMR (100 MHz, DMSO-$d_6$) δ ppm 34.59, 37.87, 38.06, 42.44, 45.46, 49.02, 51.69, 52.70, 57.21, 60.28, 98.07, 115.26, 116.24, 120.37, 128.59, 129.28, 134.24, 136.70, 138.63, 143.17, 148.46, 152.60, 154.40, 156.10, 158.59, 158.90, 166.05; HRMS (ESI): calcd for $C_{30}H_{34}N_9O_2$, 552.2835; found 552.2838.

*5.2.12.3. (E)-4-(4-amino-1-(2-(2-cyano-3-cyclopropylacryloyl)octahy-drocyclopenta[c] pyrrol-5-yl)-1H-pyrazolo[3,4-d]pyrimidin-3-yl)-N-(pyridin-2-yl)benzamide (14t).* White solid; 56 % isolated yield; Purity 98.50 %; m.p > 220 °C; $^1$H NMR (400 MHz, CDCL$_3$) δ ppm 0.95–0.98 (m, 2H), 1.26–1.30 (m, 2H), 1.48–1.53 (m, 1H), 2.11–2.19 (m, 2H), 2.52–2.59 (m, 2H), 3.12–3.18 (m, 2H), 3.54–3.68 (m, 2H), 3.88–4.01 (m, 2H), 5.41 (bs, 2H), 5.57–5.59 (m, 1H), 6.86 (d, *J* = 11.6 Hz, 1H), 7.17–7.20 (m, 1H), 7.78 (d, *J* = 8.4 Hz, 2H), 7.85–7.87 (m, 1H), 8.18–8.22 (m,3H), 8.26 (s, 1H), 8.40–8.41 (m, 1H), 10.61 (s, 1H). $^{13}$C NMR (100 MHz, DMSO-$d_6$) δ ppm 7.21, 7.29, 8.58, 37.81, 38.19, 41.17, 41.62, 50.87, 53.71, 57.69, 98.17, 105.41, 115.20, 115.71, 120.39, 128.58, 129.21, 134.24, 136.72, 138.65, 143.10, 151.84, 152.61, 154.40, 156.11, 158.62, 160.21, 166.04. 171.43; HRMS (ESI): calcd for $C_{31}H_{30}N_9O_2$, 560.2522; found 560.2521.

*5.2.12.4. 4-(4-amino-1-(2-propioloyloctahydrocyclopenta[c]pyrrol-5-yl)-1H-pyrazolo[3,4-d]pyrimidin-3-yl)-N-(pyridin-2-yl)benzamide (14u).* White solid; 45 % isolated yield; m.p > 220 °C; $^1$H NMR (400 MHz, DMSO-$d_6$) δ ppm 2.01–2.05 (m, 2H), 2.31–2.36 (m, 2H), 3.04–3.05 (m, 2H), 3.27–3.28 (m, 1H), 3.48 (s, 1H), 3.52–3.55 (m, 2H), 3.75–3.79 (m, 1H), 5.42–5.44 (m, 1H), 7.17–7.20 (m, 1H), 7.79 (d, *J* = 8.4 Hz, 2H), 7.86–7.87 (m, 1H), 8.18–8.23 (m,3H), 8.26 (s, 1H), 8.40–8.41 (m, 1H), 10.87 (s, 1H). $^{13}$C NMR (100 MHz, DMSO-*d6*) δ ppm 37.80, 38.20, 41.13, 41.64, 50.83, 53.69, 57.37, 74.81, 81.29, 97.96, 115.25, 120.38, 128.58, 129.24, 134.27, 136.70, 138.62, 143.12, 148.14, 151.84, 152.64, 154.37, 156.17, 158.66, 166.02; HRMS (ESI): calcd for $C_{27}H_{25}N_8O_2$, 493.2100; found 493.2100.

*5.2.12.5. 4-(4-amino-1-(2-(vinylsulfonyl)octahydrocyclopenta[c]pyrrol-5-yl)-1H-pyrazolo[3,4-d]pyrimidin-3-yl)-N-(pyridin-2-yl)benzamide (14r).* To the solution of **13b** (150 mg, 0.341 mmol), in DCM (5 mL) was added triethyl amine (0.142 mL, 1.022 mmol). The reaction was cooled at −50 °C, followed by dropwise addition of 2-chloroethanesulfonyl chloride (83 mg, 0.511 mmol). The reaction mixture was ambiently taken at room temperature and stirred for 3 h. The mixture was diluted with water (5 mL), stirred for 5 min., organic layer was separated and aqueous layer was extracted with DCM (2 × 5 mL). Combined organic layer was washed with brine (5 mL), dried over Na$_2$SO$_4$ and concentrated *in vacuo*. The obtained crude product was purified by preparative HPLC. White solid; 53 % yield; Purity 98.40 %; m.p > 220 °C; $^1$H NMR (400 MHz, DMSO-$d_6$) δ ppm 1.95–2.02 (m, 2H), 2.32–2.34 (m, 2H), 3.00–3.04 (m, 4H), 3.24–3.29 (m, 2H), 5.42–5.43 (m, 1H), 6.15 (d, *J* = 16.8 Hz, 1H), 6.22 (d, *J* = 10 Hz, 1H), 6.90 (dd, *J* = 16.4, 10.0 Hz, 1H),

7.16–7.11 (m, 1H), 7.77 (d, *J* = 8.4 Hz, 2H), 7.84–7.88 (m, 1H), 8.21 (d, *J* = 8.4 Hz, 2H), 8.22–8.24 (m, 1H) 8.26 (s, 1H), 8.40–8.41 (m, 1H), 10.84 (s, 1H). $^{13}$C NMR (100 MHz, DMSO-$d_6$) δ ppm 37.76, 38.14, 41.13, 41.60, 50.71, 53.59, 57.33, 97.99, 115.21, 115.83, 120.38, 128.58, 129.24, 135.08, 136.74, 138.62, 143.15, 151.89, 152.62, 154.39, 156.08, 158.58, 166.00; HRMS (ESI): calcd for $C_{26}H_{27}N_8O_3S$, 531.1927; found 531.1925.

## 5.3. BTK enzyme inhibition assay and kinase selectivity assay

The enzymatic activities of tested compounds were assessed in a cell-free enzyme assay. Briefly, fixed amount of recombinant purified human BTK (3 ng/reaction) was incubated with increasing concentration of test compounds (0.01 nmol/L to10 µmol/L) in 1X kinase reaction buffer (40 mmol/L Tris-Cl, pH 7.5,20 mmol/L MgCl$_2$, 2 mmol/L MnCl$_2$, 0.1 mg/mL BSA and 50 µmol/L DTT). Enzymatic reaction was initiated by adding a substrate cocktail containing 50 µmol/L of ATP (final concentration) and 5 µg of polyGln$_4$Tyr$_1$ in 96 well plates. The reaction was incubated at room temperature for 2 h followed by quantification of the left over ATP according to the manufacturer's protocol, using ADP-Glo reagent. Data were plotted taking 'enzyme with no inhibitor' as the 100 % kinase activity. All the experiments were performed in duplicate. The IC$_{50}$ values were calculated using linear regression analysis. The Kinase selectivity of 14b was conducted at ProQuinase (GmbH). A radiometric protein kinase assay was used in 96 well FlashPlates$^{TM}$ from Perkin Elmer.

## 5.4. TMD8 cell anti proliferation assay

TMD8 cells were routinely grown in RPMI-1640, with 10 % FBS and supplemented with 55 µmol/L β-mercapto ethanol (β-ME). For cyto-toxicity assay, defined numbers of cells were incubated in 96 well plates with increasing concentration of test compounds (0.01 nmol/L to10 µmol/L), formulated in 100 % DMSO (final concentration of DMSO in the well is 0.2 %) for 96 h. Cell growth was measured using MTT assay and IC$_{50}$ values were determined by nonlinear regression using the GraphPad Prism 6 software.

## 5.5. BMX and TEC nano BRET target engagement intracellular kinase assay

The NanoBRET target engagement assay employs an energy transfer technique designed to measure molecular proximity in living cells. The assay measures the apparent affinity of test compounds by competitive displacement of the NanoBRET tracer, reversibly bound to a NanoLuc luciferase-kinase fusion construct in cells. HEK293 (human epithelial cell line from ATCC) cells transiently expressing NanoLuc-BMX or TEC Fusion Vector were seeded into the wells of 384-well plates. The cells were pre-treated with the NanoBRET Tracer K-4 and then treated with 14b for 1 h (assay conducted at Reaction biology, Europe GmbH, Germany). The BRET signal was measured on an Envision 2104 Multilabel Reader. IC$_{50}$ value was calculated and IC$_{50}$ curve was plotted using the GraphPad Prism 4 program based on a sigmoidal dose response equation.

## 5.6. Pharmacokinetic (PK) studies

*In vivo* PK studies of target compounds and IBR were performed in male BALB/c mice, and Wister rats, using parallel study design (n = 3 per group). The oral dose was administered via gavage under overnight fasted condition and intravenous dose was administered as a bolus via tail vein injection under non fasted condition. The oral dosing in either mice or rats was performed by a homogenous suspension formulation, prepared in 1 % Tween- 80 and 0.5 % methyl cellulose in purified water. The intravenous solution was prepared in 10 % NMP, 5 % ethanol, and 85 % citric acid, in purified water. Blood samples were collected serially

from each animal at 0 h (pre-dose), 0.25, 0.5, 1, 2, 4, 6, 8, 24, 48, and 72 h post-dose. The blood samples were centrifuged to obtain plasma samples which were stored below − 70 °C. The concentrations of compounds in plasma were determined by the LC-MS/MS (Shimadzu LC10AD, USA), using YMC hydrosphere C18 (2.0 × 50 mm, 3 μm) column (YMC Inc., USA). PK parameters were derived using the non-compartmental analysis (NCA) module of WinNonlin® software.

### 5.7. In vivo efficacy studies

The *in vivo* efficacy studies were carried out in rats and mice. All animals were quarantined in the animal house of Zydus Research Centre for a 7 days period with 12 h dark/light cycle. During this period the animals had free access to standard pellet feed and water ad libitum. The experiment protocols were approved by the Committee for the Purpose of Control and Supervision of Experimentation on Animals (CPCSEA), Government of India and Institutional Animal Ethics Committee (IAEC), Zydus Research Centre.

#### 5.7.1. Protocol for TMD8 xenograft model studies

The xenograft studies were conducted in 6–8-week-old SCID mice. A total of $10 \times 10^6$ TMD-8 cells was suspended in 200 μL of phosphate buffer saline and subcutaneously injected into the flank. When tumors were palpable, animals were grouped so that the average tumor volume was around 100 mm$^3$. They were assigned to four groups: vehicle and three groups for 14b treatment (1.5, 3 & 15 mg/kg, BID) and treatment was continued for 20 days. The length and width of the tumor were measured using a digital caliper, and the volume of the tumor was calculated using the formula: length × (width)$^2$/2.

#### 5.7.2. Protocol for CIA model studies

DBA1/J male mice, 8–10 weeks old, were immunized on day 0 and 21 for induction of arthritis with bovine type II collagen, via intradermal injection, at the base of the tail. Injection volumes were 0.1 mL aliquots, consisting of a 1:1 (v/v) emulsion of *Mycobacterium tuberculosis* (2 mg/ mL in mineral oil) and bovine type II collagen (2 mg/mL in 10 mmol/L acetic acid). 14b (0.125, 0.25, 0.5 and 1 mg/kg) and IBR (0.6 mg/kg) were administered orally once a day for 4 weeks. Clinical and histological scores, an index of arthritis, were assessed according to Scales HE et al. [41], using the following criteria: 0, normal with no swelling or redness; 1, swelling and/or redness of paw or one joint; 2, swelling in two or more joints; 3, gross swelling of paw with more than two joints involved; and 4, severe arthritis of entire paw and joints.

### 5.8. Molecular docking analysis

To explain the potent and selective BTK inhibitory activity of designed molecules, docking studies were carried out using CovDock [39], a covalent docking program developed by Schrödinger. This mimics the multi-step binding process of covalent modifiers by simulating both pre- and post-reactive states. The geometry of compounds to be docked was subsequently optimized using the LigPrep [40]. The scoring function, binding mode and H-bonds were used to assess the binding affinity of the compounds. The BTK crystal structure was retrieved from the RCSB Protein Data Bank (PDB ID: 5P9M). The active site was defined to include residues within 5 A° to any of the IBR atoms. All these molecules (IBR, 9e and 14b) use an electrophilic warhead to covalently react with Cys481.

### Declaration of Competing Interest

The authors declare that they have no known competing financial interests or personal relationships that could have appeared to influence the work reported in this paper.

### Data availability

Data will be made available on request.

### References

[1] J.M. Bradshaw, The Src, Syk, and Tec family kinases: distinct types of molecular switches, Cell Signal 22 (8) (2010) 1175–1184, https://doi.org/10.1016/j. cellsig.2010.03.001.

[2] J. Rip, E.K. van der Ploeg, R.W. Hendriks, O.B.J. Corneth, The role of Bruton's tyrosine kinase in immune cell signaling and systemic autoimmunity, Crit. Rev. Immunol. 38 (1) (2018) 17–62, https://doi.org/10.1615/ CritRevImmunol.2018025184.

[3] O.B.J. Corneth, R.G.J. Klein Wolterink, R.W. Hendriks, BTK signaling in B cell differentiation and autoimmunity, Curr. Top. Microbiol. Immunol. 393 (2015) 67–105, https://doi.org/10.1007/82_2015_478.

[4] J.K. Chung, L.M. Nocka, A. Decker, Q. Wang, T.A. Kadlecek, A. Weiss, J. Kuriyan, J. T. Groves, Switch-like activation of Bruton's tyrosine kinase by membrane-mediated dimerization, Proc. Natl. Acad. Sci. U. S. A. 116 (22) (2019) 10798–10803, https://doi.org/10.1073/pnas.1819309116.

[5] C. Brunner, B. Müller, T. Wirth, Bruton's tyrosine kinase is involved in innate and adaptive immunity, Histol. Histopathol. 20 (3) (2005) 945–955. https://doi.org/ 10.14670/HH-20.945.

[6] L.A. Honigberg, A.M. Smith, M. Sirisawad, E. Verner, D. Loury, B. Chang, S. Li, Z. Pan, D.H. Thamm, R.A. Miller, J.J. Buggy, The Bruton tyrosine kinase inhibitor PCI-32765 blocks B-cell activation and is efficacious in models of autoimmune disease and B-cell malignancy, Proc. Natl. Acad. Sci. U. S. A. 20, 107(29) (2010) 13075–13080, https://doi.org/10.1073/pnas.1004594107.

[7] D. Xu, Y. Kim, J. Postelnek, M.D. Vu, D.Q. Hu, C. Liao, M. Bradshaw, J. Hsu, J. Zhang, A. Pashine, D. Srinivasan, J. Woods, A. Levin, A. O'Mahony, T.D. Owens, Y. Lou, R.J. Hill, S. Narula, J. deMartino, J.S. Fine, RN486, a selective bruton's tyrosine kinase inhibitor, abrogates immune hypersensitivity responses and arthritis in rodents, J. Pharmacol. Exp. Ther. 341 (1) (2012) 90–103, https://doi. org/10.1124/jpet.111.187740.

[8] J.A. Di Paolo, T. Huang, M. Balazs, J. Barbosa, K.H. Barck, B.J. Bravo, R.A. D. Carano, J. Darrow, D.R. Davies, L.E. DeForge, L. Diehl, R. Ferrando, S.L. Gallion, A.M. Giannetti, P. Gribling, V. Hurez, S.G. Hymowitz, R. Jones, J.E. Kropf, W. P. Lee, P.M. Maciejewski, S.A. Mitchell, H. Rong, B.L. Staker, J.A. Whitney, S. Yeh, W.B. Young, C. Yu, J. Zhang, K. Reif, K.S. Currie, Specific Btk inhibition suppresses B cell- and myeloid cell-mediated arthritis, Nat. Chem. Biol. 7 (1) (2011) 41–50.

[9] A.L. Rankin, N. Seth, S. Keegan, T. Andreyeva, T.A. Cook, J. Edmonds, N. Mathialagan, M.J. Benson, J. Syed, Y. Zhan, S.E. Benoit, J.S. Miyashiro, N. Wood, S. Mohan, E. Peeva, S.K. Ramaiah, D. Messing, B.L. Homer, K. Dunussi-Joannopoulos, C.L. Nickerson-Nutter, M.E. Schnute, J. Douhan, Selective inhibition of BTK prevents murine lupus and antibody-mediated glomerulonephritis, J. Immunol. 191 (9) (2013) 4540–4550.

[10] K.M. Gillooly, C. Pulicicchio, M.A. Pattoli, L. Cheng, S. Skala, E.M. Heimrich, K. W. McIntyre, T.L. Taylor, D.W. Kukral, S. Dudhgaonkar, J. Nagar, D. Banas, S. H. Watterson, J.A. Tino, A. Fura, J.R. Burke, S.V. Reddy, Bruton's tyrosine kinase inhibitor BMS-986142 in experimental models of rheumatoid arthritis enhances efficacy of agents representing clinical standard-of-care, PLoSOne. 12 (7) (2017) e0181782.

[11] J.J. Crawford, A.R. Johnson, D.L. Misner, L.D. Belmont, G. Castanedo, R. Choy, M. Coraggio, L. Dong, C. Eigenbrot, R. Erickson, N. Ghilardi, J. Hau, A. Katewa, P.B. Kohli, W. Lee, J.W. Lubach, B.S. McKenzie, D.F. Ortwine, L. Schutt, S. Tay, B. Wei, K. Reif, L. Liu, H. Wong, W.B. Young, Discovery of GDC-0853: a potent, selective, and non covalent Bruton's tyrosine kinase inhibitor in early clinical development. J. Med. Chem. 2018, 61, 2227–2245. https://doi.org/10.1021/acs. jmedchem.7b01712.

[12] P. Haselmayer, M. Camps, L. Liu-Bujalski, N. Nguyen, F. Morandi, J. Head, A. O'Mahony, S.C. Zimmerli, L. Bruns, A.T. Bender, P. Schroeder, R. Grenningloh, Efficacy and pharmacodynamic modeling of the BTK Inhibitor Evobrutinib in autoimmune disease models, J. Immunol. 202 (2019) 2888–2906, https://doi.org/ 10.4049/jimmunol.1800583.

[13] R.W. Hendriks, S. Yuvaraj, L.P. Kil, Targeting Bruton's tyrosine kinase in B cell malignancies, Nat. Rev. Cancer 14 (2014) 219–232, https://doi.org/10.1038/ nrc3702.

[14] J.C.W. Edwards, G. Cambridge, Prospects for B-cell-targeted therapy in autoimmune disease, Rheumatology 44 (2005) 151–156, https://doi.org/10.1093/ rheumatology/keh446.

[15] J.C.W. Edwards, G. Cambridge, B-cell targeting in rheumatoid arthritis and other autoimmune diseases, Nat. Rev. Immunol. 6 (5) (2006) 394–403.

[16] Z. Pan, H. Scheerens, S.J. Li, B.E. Schultz, P.A. Sprengeler, L.C. Burrill, R. V. Mendonca, M.D. Sweeney, K.C. Scott, P.G. Grothaus, D.A. Jeffery, J.M. Spoerke, L.A. Honigberg, P.R. Young, S.A. Dalrymple, J.T. Palmer, Discovery of selective

irreversible inhibitors for Bruton's tyrosine kinase, ChemMedChem 2 (1) (2007) 58–61, https://doi.org/10.1002/cmdc.200600221.

[17] US Food and Drug Administration. Approved Drugs: Ibrutinib. Available at: https://wayback.archiveit.org/7993/20170111231706/http://www.fda.gov/Drugs/InformationOnDrugs/ApprovedDrugs/ucm374857.htm.

[18] R. de Vries, J.W. Smit, P. Hellemans, J. Jiao, J. Murphy, D. Skee, J. Snoeys, J. Sukbuntherng, M. Vliegen, L. de Zwart, E. Mannaert, J. de Jong, Stable isotope-labelled intravenous microdose for absolute bioavailability and effect of grapefruit juice on ibrutinib in healthy adults, Br. J. Clin. Pharmacol. 81 (2) (2016) 235–245.

[19] E.D. Eisenmann, Q. Fu, E.M. Muhowski, Y. Jin, M.E. Uddin, D.A. Garrison, R.H. Weber, J.A. Woyach, J.C. Byrd, A. Sparreboom, S.D. Baker, Intentional Modulation of Ibrutinib Pharmacokinetics through CYP3A Inhibition. Cancer Research Communications. 2021, 1(2), 79–89. https://doi.org/10.1158/2767-9764.CRC-21-0076.

[20] R.R. Furman, S. Cheng, P. Lu, M. Setty, A.R. Perez, A. Guo, et al. Ibrutinib resistance in chronic lymphocytic leukemia. N Engl J Med. 2014, 370, 2352–2354. https://doi.org/10.1056/NEJMc1402716.

[21] J.C. Byrd, B.H. Harrington, S. O'Brien, J.A. Jones, A.S. Schuh, S. Devereux, J. Chaves, W.G. Wierda, F.T. Awan, J.R. Brown, P. Hillmen, D.M. Stephens, P. Ghia, J.C. Barrientos, J.M. Pagel, J. Woyach, D. Johnson, J. Huang, X.L. Wang, A. Kaptein, B.J. Lannutti, T. Covey, M. Fardis, J. McGreivy, A. Hamdy, W. Rothbaum, R. Izumi, T.G. Diacovo, A.J. Johnson, R.R. Furman, Acalabrutinib (ACP-196) in relapsed chronic lymphocytic leukemia. N. Engl. J. Med. 2016, 374, 323–332. https://doi.org/10.1056/NEJMoa1509981.

[22] Y. Sawalha, D.A. Bond, L. Alinari, Evaluating the therapeutic potential of Zanubrutinib in the treatment of relapsed/refractory mantle cell lymphoma: evidence to date, OncoTargets and Therapy. 13 (2020) 6573–6581, https://doi.org/10.2147/OTT.S238832.

[23] Jr T.J. Lynch, E.S. Kim, B. Eaby, J. Garey, D.P. West, M.E. Lacouture, Epidermal growth factor receptor inhibitor-associated cutaneous toxicities: an evolving paradigm in clinical management. Oncologist. 2007, 12(5), 610-21. https://doi.org/theoncologist.12-5-610.

[24] A. Alsadhan, J. Cheung, M. Gulrajani, E.M. Gaglione, P. Nierma, A. Hamdy, R. Izumi, E. Bibikova, P. Patel, C. Sun, T. Covey, S.E.M. Herman, A. Wiestner, Pharmacodynamic Analysis of BTK Inhibition in Patients with Chronic Lymphocytic Leukemia Treated with Acalabrutinib, Clin. Cancer Res. 2020, 26 (12), 2800-2809. https://doi.org/10.1158/1078-0432.CCR-19-3505.

[25] T.Y. Estupiñán, A. Berglöf, R. Zain, C.I.E. Smith, Comparative Analysis of BTK Inhibitors and Mechanisms Underlying Adverse Effects, Front. Cell Dev. Biol. 9 (2021), 630942, https://doi.org/10.3389/fcell.2021.630942.

[26] S. Dhillon, Tirabrutinib: first approval, Drugs. 80 (8) (2020) 835–840, https://doi.org/10.1007/s40265-020-01318-8.

[27] S.H. Watterson, Q.J. Liu, M.B Bertrand, D.G. Batt, L. Li, M.A. Pattoli, S. Skala, L.H. Cheng, M.T. Obermeier, R. Moore, Z. Yang, R. Vickery, P.A. Elzinga, L. Discenza, C. D'Arienzo, K.M. Gillooly, T.L. Taylor, C. Pulicicchio, Y.F. Zhang, E. Heimrich, K.W. McIntyre, Q. Ruan, R.A. Westhouse, I.M. Catlett, N.Y. Zheng, C. Chaudhry, J. Dai, M.A. Galella, A.J. Tebben, M. Pokross, J.Q. Li, R.L. Zhao, D. Smith, R. Rampulla, A. Allentoff, M.A. Wallace, A. Mathur, L. Salter-Cid, J.E. Macor, P.H. Carter, A. Fura, J.M. Burke, J.A. Tino, Discovery of Branebrutinib (BMS-986195): a Strategy for Identifying a highly potent and selective covalent inhibitor providing rapid *in vivo* inactivation of Bruton's tyrosine kinase (BTK), J. Med. Chem. 2019, 62, 3228–3250. https://doi.org/10.1021/acs.jmedchem.9b00167.

[28] D. Isenberg, R. Furie, N.S. Jones, P. Guibord, J. Galanter, C. Lee, A. McGregor, B. Toth, J. Rae, O. Hwang, R. Desai, A. Lokku, N. Ramamoorthi, J.A. Hackney, P. Miranda, V.A. de Souza, J.J. Jaller-Raad, A. Maura Fernandes, R. Garcia Salinas, L.W. Chinn, M.J. Townsend, A.M. Morimoto, K. Tuckwell, Efficacy, safety, and pharmacodynamic effects of the Bruton's tyrosine kinase inhibitor Fenebrutinib (GDC-0853) in systemic lupus erythematosus: results of a phase II, randomized, double-blind, placebo-controlled trial, Arthritis Rheumatol. 73 (10) (2021) 1835–1846, https://doi.org/10.1002/art.41811.

[29] J. Singh, R.C. Petter, T.A. Baillie, A. Whitty, The Resurgence of Covalent Drugs, Nat. Rev. Drug Discov. 10 (2011) 307–317, https://doi.org/10.1038/nrd3410.

[30] A.S. Kalgutkar, D.K. Dalvie, Drug discovery for a new generation of covalent drugs, Expert Opin. Drug Discov. 7 (2012) 561–581, https://doi.org/10.1517/17460441.2012.688744.

[31] Q. Liu, Y. Sabnis, Z. Zhao, T. Zhang, S.J. Buhrlage, L.H. Jones, N.S. Gray, Developing irreversible inhibitors of the protein kinase cysteinome, Chem. Biol. 20 (2013) 146–159, https://doi.org/10.1016/j.chembiol.2012.12.006.

[32] Y. Yin, C. Chen, R. Yu, L. Shu, T. Zhang, D. Zhang, Discovery of novel selective Janus kinase 2 (JAK2) inhibitors bearing a 1H-pyrazolo[3,4-d]pyrimidin-4-amino scaffold, Bioorg. Med. Chem. 27 (8) (2019) 1562–1576, https://doi.org/10.1016/j.bmc.2019.02.054.

[33] 6a-h were prepared according reported literature procedures, vis procedure mentioned in (i) B. Deng, X. Li, B.Wang, Z. Zhu, 3-cyan-6-aminoquinoline derivatives, preparation method there of and application there of in medicines, CN102146084A. (ii) J.C. Pelletier, L. Felix, D.M. Green, et al. Naphthylpyrimidine, naphthylpyrazine and naphthylpyridazine analogs and their use as agonists of the Wnt-beta-catenin cellular messaging system, WO2009/026326. (iii) P.K. Sasamal, S. Ahmed, G. Prabhu, et al. Substituted hetrocyclic compound as Tropomyocin receptor kinase A (TRKA) inhibitors, WO 2013/088257. (iv) J. Hert, D. Hunziker, P. Mattei, et al. New bicyclic derivatives, WO 2014/048865. (v) J. Finn, L.W. Tari, Z. Chen, et al.Tricyclic gyrase inhibitors, WO2015038661A1. (vi) H. Chobanian, B. Pio, Y. Guo, et al. Inhibitors of the renal outer medullary channel, WO 2015/095097. (vii) Brameld, E. Verner, Quinolone derivatives as fibroblast growth factor receptor inhibitors, WO 2016/191172. (viii) Q. Li, J. Zhang, S. Jian, A. Li, W. Xu, Heterocyclic compound as kinase inhibitors, compositions comprising the heterocyclic compound, and methods of use thereof, WO 2020/248972.

[34] Y.S. Kiani, I. Jabeen, Lipophilic Metabolic Efficiency (LipMetE) and Drug Efficiency Indices to Explore the Metabolic Properties of the Substrates of Selected Cytochrome P450 Isoforms, ACS Omega 5 (1) (2020) 179–188, https://doi.org/10.1021/acsomega.9b02344.

[35] K. Ghoshdastidar, H. Patel, H. Bhayani, A. Patel, K. Thakkar, D. Patel, M. Sharma, J. Singh, J. Mohapatra, A. Chatterjee, D. Patel, R. Bahekar, R. Sharma, L. Gupta, N. Patel, P. Giri, N.R. Srinivas, M. Jain, D. Bandyopadhyay, P.R. Patel, R.C. Desai, ZYBT1, a potent, irreversible Bruton's tyrosine kinase (BTK) inhibitor that inhibits the C481S BTK with profound efficacy against arthritis and cancer, Pharmacol. Res. Perspect. 8 (4) (2020) e00565, https://doi.org/10.1002/prp2.565.

[36] Y. Zhao, Y. Liu, D. Zhou, Q. Dai, S. Liu, Anti-arthritic effect of chebulanin on collagen- induced arthritis in mice. PLoSONE.2015, 1–14. https://doi.org/10.1371/journal.pone.0139052.

[37] A. Oda, Y. Ikeda, H.D. Ochs, B.J. Druker, K. Ozaki, M. Handa, T. Ariga, Y. Sakiyama, O.N. Witte, M.I. Wahl, Rapid tyrosine phosphorylation and activation of Bruton's tyrosine/Tec kinases in platelets induced by collagen binding or CD32 cross-linking, Blood 95 (5) (2000) 1663–1670, https://doi.org/10.1182/blood.V95.5.1663.005k44_1663_1670.

[38] M. Forster, X.J. Liang, M. Schröder, S. Gerstenecker, A. Chaikuad, S. Knapp, S. Laufer, M. Gehringer, Discovery of a Novel Class of Covalent Dual Inhibitors Targeting the Protein Kinases BMX and BTK, Int. J. Mol. Sci. 21 (23) (2020) 9269, https://doi.org/10.3390/ijms21239269.

[39] K. Zhu, K.W. Borrelli, J.R. Greenwood, T. Day, R. Abel, R.S. Farid, E. Harder, Docking covalent inhibitors: a parameter free approach to pose prediction and scoring, J. Chem. Inf. Model. 54 (7) (2014) 1932–1940, https://doi.org/10.1021/ci500118s.

[40] Schrödinger Release, 2019-1: LigPrep, Schrödinger, LLC, New York, NY, 2019.

[41] H.E. Scales, M. Ierna, K.M. Smith, et al. Assessment of murine collagen- induced arthritis by longitudinal non-invasive duplexed molecular optical imaging. Rheumatology. 2016, 55, 564-572. https://doi.org/10.1093/rheumatology/kev361.